(2)

NAVAL POSTGRADUATE SCHOOL

Monterey, California

THESIS

SYSTEM ANALYSIS OF A TACTICAL
MULTI-SATELLITE
COMMUNICATION SYSTEM

by

Thomas M. Clemons, III

December 1989

Thesis Advisor Tri T. Ha

Unclassified

security classification of this page

REPORT DOCUMENTATION PAGE

1a Report Security Classification: Unclassified	1b Restrictive Markings
2a Security Classification Authority	3 Distribution/Availability of Report: Approved for public release; distribution is unlimited.
2b Declassification Downgrading Schedule	
4 Performing Organization Report Number(s)	5 Monitoring Organization Report Number(s)
6a Name of Performing Organization: Naval Postgraduate School; 6b Office Symbol (*if applicable*): code 39	7a Name of Monitoring Organization: Naval Postgraduate School
6c Address (*city, state, and ZIP code*): Monterey, CA 93943-5000	7b Address (*city, state, and ZIP code*): Monterey, CA 93943-5000
8a Name of Funding Sponsoring Organization; 8b Office Symbol (*if applicable*)	9 Procurement Instrument Identification Number
8c Address (*city, state, and ZIP code*)	10 Source of Funding Numbers: Program Element No; Project No; Task No; Work Unit Accession No

11 Title (*Include security classification*) SYSTEM ANALYSIS OF A TACTICAL MULTI-SATELLITE COMMUNICATION SYSTEM (Unclassified)

12 Personal Author(s) Thomas M. Clemons, III

13a Type of Report	13b Time Covered	14 Date of Report (*year, month, day*)	15 Page Count
Master's Thesis	From To	December 1989	86

16 Supplementary Notation The views expressed in this thesis are those of the author and do not reflect the official policy or position of the Department of Defense or the U.S. Government.

17 Cosati Codes			18 Subject Terms (*continue on reverse if necessary and identify by block number*)
Field	Group	Subgroup	Frequency hopping, MFSK, Fading, Low Altitude Satellites

19 Abstract (*continue on reverse if necessary and identify by block number*)

Initial design study of a low altitude satellite (LASAT) communication system is performed. The use of many inexpensive, low-altitude satellites in random orbits may be a solution to vulnerability of current military communication systems. Statistical study of orbit characteristics is performed giving the mean number of satellites in view of a ground station and the coverage density of the satellite array. Waveform analysis is performed on a coded and uncoded, orthogonal, noncoherent, fast-frequency-hopped M-ary frequency-shift-keyed signal in a Rician fading channel with optimum partial band jamming. An analytical expression for the system probability of bit error is obtained and numerical results are generated for various levels of fading, jamming, and diversity. Forward error correction coding is applied using convolutional codes and Reed-Solomon codes.

20 Distribution Availability of Abstract	21 Abstract Security Classification	
☒ unclassified unlimited ☐ same as report ☐ DTIC users	Unclassified	
22a Name of Responsible Individual: Tri T. Ha	22b Telephone (*Include Area code*): (408) 646-2788	22c Office Symbol: code 62ha

DD FORM 1473,84 MAR 83 APR edition may be used until exhausted
All other editions are obsolete

security classification of this page

Unclassified

Approved for public release; distribution is unlimited.

System Analysis of a Tactical Multi-Satellite
Communication System

by

Thomas M. Clemons, III
Lieutenant, United States Navy
B.S.E.E., United States Naval Academy, 1982.

Submitted in partial fulfillment of the
requirements for the degrees of

MASTER OF SCIENCE IN ELECTRICAL ENGINEERING
and
ELECTRICAL ENGINEER

from the

NAVAL POSTGRADUATE SCHOOL
December 1989

Author: _____
Thomas M. Clemons, III

Approved by: _____
Tri T. Ha, Thesis Advisor

_____
Glen A. Myers, Second Reader

_____
John P. Powers, Chairman,
Department of Electrical and Computer Engineering

_____
Gordon E. Schacher,
Dean of Science and Engineering

ABSTRACT

Initial design study of a low altitude satellite (LASAT) communication system is performed. The use of many inexpensive, low-altitude satellites in random orbits may be a solution to vulnerability of current military communication systems. Statistical study of orbit characteristics is performed giving the mean number of satellites in view of a ground station and the coverage density of the satellite array. Waveform analysis is performed on a coded and uncoded, orthogonal, noncoherent, fast-frequency-hopped M-ary frequency-shift-keyed signal in a Rician fading channel with optimum partial band jamming. An analytical expression for the system probability of bit error is obtained and numerical results are generated for various levels of fading, jamming, and diversity. Forward error correction coding is applied using convolutional codes and Reed-Solomon codes.

TABLE OF CONTENTS

I. INTRODUCTION 1

II. BACKGROUND INFORMATION 2
A. LOW-ALTITUDE SATELLITES 2
B. THE FADING CHANNEL 2
C. FREQUENCY HOPPING SPREAD SPECTRUM 6
D. SUMMARY OF RESEARCH 7
1. Orbit statistics 8
2. Waveform selection 9

III. LASAT SYSTEM 10
A. DISTRIBUTION OF LASAT 10
1. Theoretical development 10
2. Numerical simulation 14
B. COVERAGE 18
1. Theoretical development 18
2. Numerical simulation 23

IV. WAVEFORM ANALYSIS 26
A. UNCODED FH/MFSK IN A RICIAN FADING CHANNEL WITH PARTIAL BAND JAMMING 26
B. CODED FH/MFSK IN A RICIAN FADING CHANNEL WITH PARTIAL BAND JAMMING 41
1. Convolutional codes 44
2. Reed-Solomon codes 45
C. NUMERICAL RESULTS 46
1. Uncoded performance 46
2. Coded performance 47

V. CONCLUSIONS AND RECOMMENDATIONS 71
A. CONCLUSIONS 71

B. RECOMMENDATIONS 71

APPENDIX 73

LIST OF REFERENCES 75

INITIAL DISTRIBUTION LIST 77

LIST OF TABLES

Table 1. MEAN AND VARIANCE OF SATELLITE DISTRIBUTION. 15
Table 2. NUMBER OF SATELLITES SEEN BY GROUND STATION 16

LIST OF FIGURES

Figure 1. Example of a multipath channel on transmitted pulses 4
Figure 2. Typical Frequency hopped spread spectrum system 8
Figure 3. Geometry of satellite orbit distribution. 12
Figure 4. Distribution of the number of satellites within view 17
Figure 5. Geometry of satellite coverage. 19
Figure 6. Example of satellite communication range. 20
Figure 7. Coverage density of satellites 25
Figure 8. FH/MFSK transmitter 28
Figure 9. FH/MFSK receiver 29
Figure 10. FH/MFSK system with coding 43
Figure 11. Performance of receiver for no fading 48
Figure 12. Performance of receiver for Rician fading 49
Figure 13. Performance of receiver for Rician fading 50
Figure 14. Performance of receiver for Rayleigh fading 51
Figure 15. Performance of receiver for Rician fading 52
Figure 16. Performance of receiver for Rayleigh fading 53
Figure 17. Performance of receiver for Rician fading 54
Figure 18. Performance of receiver for Rayleigh fading 55
Figure 19. Performance of rate 1/2 convolutional code with no fading 57
Figure 20. Performance of rate 1/2 convolutional code in Rician fading 58
Figure 21. Performance of rate 1/2 convolutional code in Rician fading 59
Figure 22. Performance of rate 1/2 convolutional code in Rayleigh fading 60
Figure 23. Performance of rate 1/2 convolutional code in Rician fading 61
Figure 24. Performance of rate 1/2 convolutional code in Rician fading 62
Figure 25. Performance of rate 1/3 convolutional code in Rician fading 63
Figure 26. Performance of rate 1/3 convolutional code in Rayleigh fading 64
Figure 27. Performance of Reed-Solomon (15,8) code in Rician fading 65
Figure 28. Performance of Reed-Solomon (15,8) code in Rayleigh fading 66
Figure 29. Performance comparision of codes with no fading 67
Figure 30. Performance comparision of codes in Rician fading 68
Figure 31. Performance comparision of codes in Rician fading 69
Figure 32. Performance comparision of codes in Rayleigh fading 70

ACKNOWLEDGMENT

I would like to thank Professor Tri T. Ha, my thesis advisor; Professor Glen A. Myers, my second reader; Professor R. Clark Robertson; and Professor Paul Moose for providing their expertise and encouragement during the completion of this thesis.

I dedicate this thesis to my wife, Martha, and my daughter, Ellen. Their unfailing patience, understanding, support, and love were an inspiration.

I. INTRODUCTION

Current U. S. military communciations are performed using a small number of highly sophisticated and expensive satellites in geostationary orbits. The loss of only a few of these satellites will have a serious impact on vital communications. Although current technology has not yet produced an anti-satellite (ASAT) system that can reach geostationary orbits, such systems may be developed in the future. In addition, ground tracking and control stations are susceptible to breakdown and attack. To close this vulnerability window many more satellites must be fielded quickly. The problem is the enormous cost of building and launching these high-altitude satellites, which is estimated at hundreds of millions of dollars each.

A possible solution to this vulnerability in times of crisis is the use of less sophisticated, low-altitude satellites designed to be launched quickly in large numbers. These satellites would be light and inexpensive to build and operate. Hundreds of these satellites would be placed in orbit to provide full earth coverage and their sheer numbers would overwhelm any ASAT system. To achieve reasonable costs, the satellites will have minimum station-keeping ability, if any. Initial system analysis has indicated that about 250 satellites in random orbits would be needed to provide full earth coverage with inplace reconstitution [Ref. 1]. The multi-satellite system (MSS) considered in Ref. 1 is primarly expected to be used as a strategic replacement to the current geostationary system and is designed to provide world-wide communications. This configuration would require that the satellites communicate between each other via a packet switching system. The system considered in this thesis is similar to the multi-satellite system of Ref. 1 but would be used for short term tactical communications. Therefore, the satellite crosslinks are unnecessary.

II. BACKGROUND INFORMATION

A. LOW-ALTITUDE SATELLITES

The main purpose of Low-Altitude Satellites (LASAT's) is to handle crisis communications for military commanders. The satellite is expected to operate with encrypted data and digitized voice links to local areas, possibly between hand-held computers in the field. One advantage of LASAT is the small propagation delay as compared to 250 ms for geostationary satellites. This will facilitate the speedy transmission of data, and many data protocols designed for terrestial radio communications can be modified for LASAT use.

On the other hand, LASAT coverage is very small, and the window of communciations will last for only minutes instead of hours. This requires a great number of satellites to provide continuous coverage. It is envisioned that LASAT's will be deployed randomly in many orbits without station-keeping capability and that communications will be through omnidirectional antennas. Such a random system requires more satellites to provide continous coverage than does one with well-defined orbits where station keeping is required. Therefore, the number of satellites seen by a ground terminal is a random variable, and a ground station signal may be received simultaneously by many satellites. Also, when used for tactical communications without cross-links, the same ground signals relayed by many LASAT's become satellite multipath signals at the receiving ground terminals with near identical power if classical transponders are used. In addition, because low-gain antennas will be used by the ground terminals and LASAT's, reflection multipath signals are also present. The combination of these multipath effects result in a fading channel.

B. THE FADING CHANNEL

Generally, radio waves do not take a direct path from the transmitter to the receiver. Terrain, buildings, vegetation, and the ionosphere cause multiple reflections and refractions of the signal. Therefore, a communications channel is,

in most cases, a multipath channel with the signals arriving at the receiver from a variety of directions and with different delays. Furtheremore, the channel is very dynamic with the movement of the ionosphere, receiver and transmitters, and foliage causing a time variance in the structure of the medium. As a result of such time variations, the multipath varies with time. Small changes in path length can also result in large phase changes in the signal at the receiver antenna.

Stein [Ref. 2] describes the system in phasor terms, where the observed received phasor is a vector sum of several phasors with each varing randomly and individually over a full 2π range. As a result, constructive and destructive interference occurs and the received signals will have different amplitudes. The fading channel, therefore, is characterized by a random time-variant impulse response. Thus, the transmission of a pulse will result in a pulse train arriving at the receiver with variations in amplitude. If a series of pulses are sent, the pulse train associated with each transmission will be different as shown in Figure 1 on page 4 [Ref. 3 : p. 704]. These time variations are unpredictable to the user and may be considered random which implies that the received signal can be modeled as a random process.

In the general case, the received signal will have both a direct (or specular) component and a number of scattered (or diffuse) components. The scattered components' arrival times and amplitudes will vary randomly about the mean provided by the direct component. As a result, the envelope of the received signal will be similar to the envelope of a non-zero mean signal. This type of channel is described as Rician. The amplitude of the received signal has the probability density function (pdf) [Ref. 4: p. 105]

$$f_A(a) = \frac{a}{\sigma^2} \exp\left\{ -\frac{a^2 + \alpha^2}{2\sigma^2} \right\} I_0\left(\frac{\alpha a}{\sigma^2} \right), \quad a > 0, \tag{2.1}$$

where α^2 represents the power of the direct component, $2\sigma^2$ is the expected value of the power of the scattered component, and $I_0(x)$ is the zeroth-order modified Bessel function of the first kind. For the case where there is no direct component

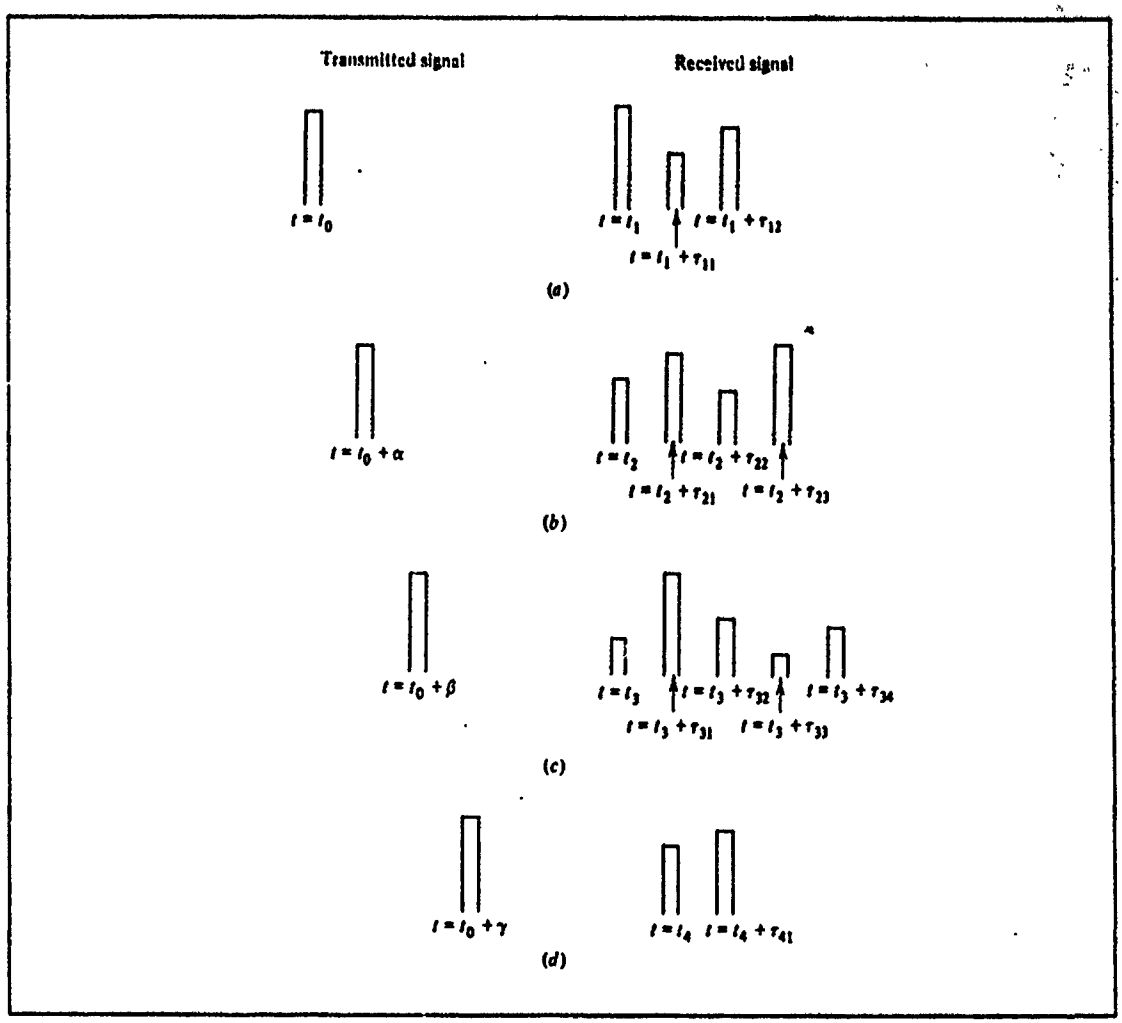

Figure 1. Example of a multipath channel on transmitted pulses: From Ref. 3: p.704.

and all the received energy is via the scattered components, the channel is described as Rayleigh with the pdf of the amplitude given by

$$f_A(a) = \frac{a}{\sigma^2} \exp\left\{ -\frac{a^2}{2\sigma^2} \right\}, \quad a > 0. \tag{2.2}$$

The fading characteristic of the channel may be rapid or slow dependent upon the relative time and frequency scale of the medium and the signal bandwidth. The coherence bandwidth is defined as a measure of the frequency

dependence of the channel. If the channel coherence bandwidth is smaller than the bandwidth of the transmitted signal, the channel is frequency-selective and the signal is severely distorted. However, if the coherence bandwidth is larger than the signaling bandwidth, the channel is frequency-nonselective, and the signal is undistorted. A slowly-fading channel is one in which the coherence time is large and the signal is unchanged over a signaling interval. On the other hand, in a rapidly-fading channel, the signal is distorted by changes in amplitude or frequency during the signaling interval.

Unusual conditions in the ionosphere can result in significant scintillations of earth/satellite links. These effects are highly frequency dependent. In mild scintillation the channel is typically Rician but at times of strong scintillation (deep fading) has been observed to be Rayleigh. The amount of scintillation is dependent upon satellite altitude, time of day, and latitude, with the largest effects near the nighttime equatorial zone. Further significant multipath effects that would be involved in a LASAT system are dependent upon terrain and the speed of the satellite and terminals. The relative speed between the satellite and the ground station can be significant with a low earth orbit satellite system, and will increase fading effects. [Ref. 2]

Diversity is one technique that can be used to overcome the effects of fading. With diversity the same information is provided over two or more independently fading channels. This lowers the probability that any individual symbol will be affected by deep fading on each channel. There are a variety of methods of diversity combining and they include the following [Ref. 2]:

- Spaced antennas
  Antenna spacing of ten wavelengths or greater can result in independent channels. This technique, however, is not well suited to satellite UHF communications because of the long wavelengths.
- Frequency diversity
  The use of wideband frequency hopping (fast hopping) on fading channels, with the same information carried on different hops, tends to result in independent states of fading.

- Multipath diversity
  A signal having a bandwidth greater than the coherence bandwidth of the channel will resolve multipath components and thus, provide the the receiver with several independent fading signal paths. This is an inherent characteristic of direct sequence spread spectrum systems.
- Time diversity
  The same data is repetitively transmitted at intervals that exceed the coherence time of the channel which results in independent fading conditions.

Coding and interleaving are other techniques which are similar to time diversity in providing redundancy. This is particularly true with binary linear block codes. However, convolutional codes and other non-binary linear codes provide satisfactory results. A more detailed coverage of fading channels is presented in Ref. 2 and 3.

C. FREQUENCY HOPPING SPREAD SPECTRUM

The previous section discussed the effects of the fading channel and indicated some methods available to overcome the resulting degradation in system performance. Fast frequency hopping spread spectrum, with the same information carried on different hops. is one form of frequency diversity that may be used. If sequential hops exceed the coherence bandwidth of the channel, then fading for each hop frequency is independent. The selection of the frequency slots in each signaling interval is made pseudo-random according to the output of a pseudo-noise generator.

Due to rapid signal phase changes which occur within a fading channel and the difficulty in building and using coherent demodulators for frequency shift keyed systems, most fast frequency hopping systems use noncoherent, orthogonal modulation schemes. A common data modulation for FH systems is M-ary frequency shift keying (MFSK) where $K = \log_2 M$ bits are used to determine which of M frequency tones will be used for carrier modulation. The tones are usually spaced far enough apart so that the transmitted signals are orthogonal. This implies that the frequency spacing be at least $1/KT_b$ Hz, where T_b is the bit duration and $T_s = KT_b$ is the duration of each symbol.

When fast frequency hopping is used with a M-ary FSK system, each of the M symbols is subdivided into L chips. At each chip, the MFSK modulator output is hopped to a different frequency. Since the chip duration T_c is shorter than the data modulator output symbol duration T_s, the minimum tone spacing for orthogonal signals is $B = 1/T_c = L/KT_b$. The total system bandwidth then becomes $W = mMB = mLM/KT_b$, where m is an arbitary integer that defines the hopping bandwidth.

A typical frequency hopping system is shown in Figure 2 on page 8. At the receiver, an identical PN generator synchronized with the received signal removes the pseudo-random frequency translation by mixing the synthesizer output with the received signal [Ref. 5]. For an orthogonal, noncoherent system, demodulation is usually accomplished through square-law, or envelope detectors. The detector output can then make a hard decision at each chip interval as to which of the M-channels contains the signal and make an estimate on all L chip decisions, or it can sum the energy of L chips on each channel and make a soft decision based on the largest value.

Although the fast frequency hopping system is effective in a fading channel, partial band jamming can seriously degrade the signal when it hops in and out of the jamming band. The partial band jammer concentrates its power over a small fraction η of the system bandwidth. On some hops, the signal will be at a frequency which is jammed, while on other hops, the signal will be at a frequency where the only interference is thermal noise. A system which can measure the amount of thermal and jamming noise power per hop can provide this side information to normalize the measurements obtained at the detector outputs (chapter IV). Worst case jamming occurs when the jammer optimizes η to maximize the system bit error probability. In system design it is normally assumed that the jammer has knowledge of the system state and is able to optimize η. Therefore, performance calculations provide an upper bound on error rates.

D. SUMMARY OF RESEARCH

This thesis covers the communications analysis of LASAT system design. Included in this study are orbit characteristics of the system, and the waveform

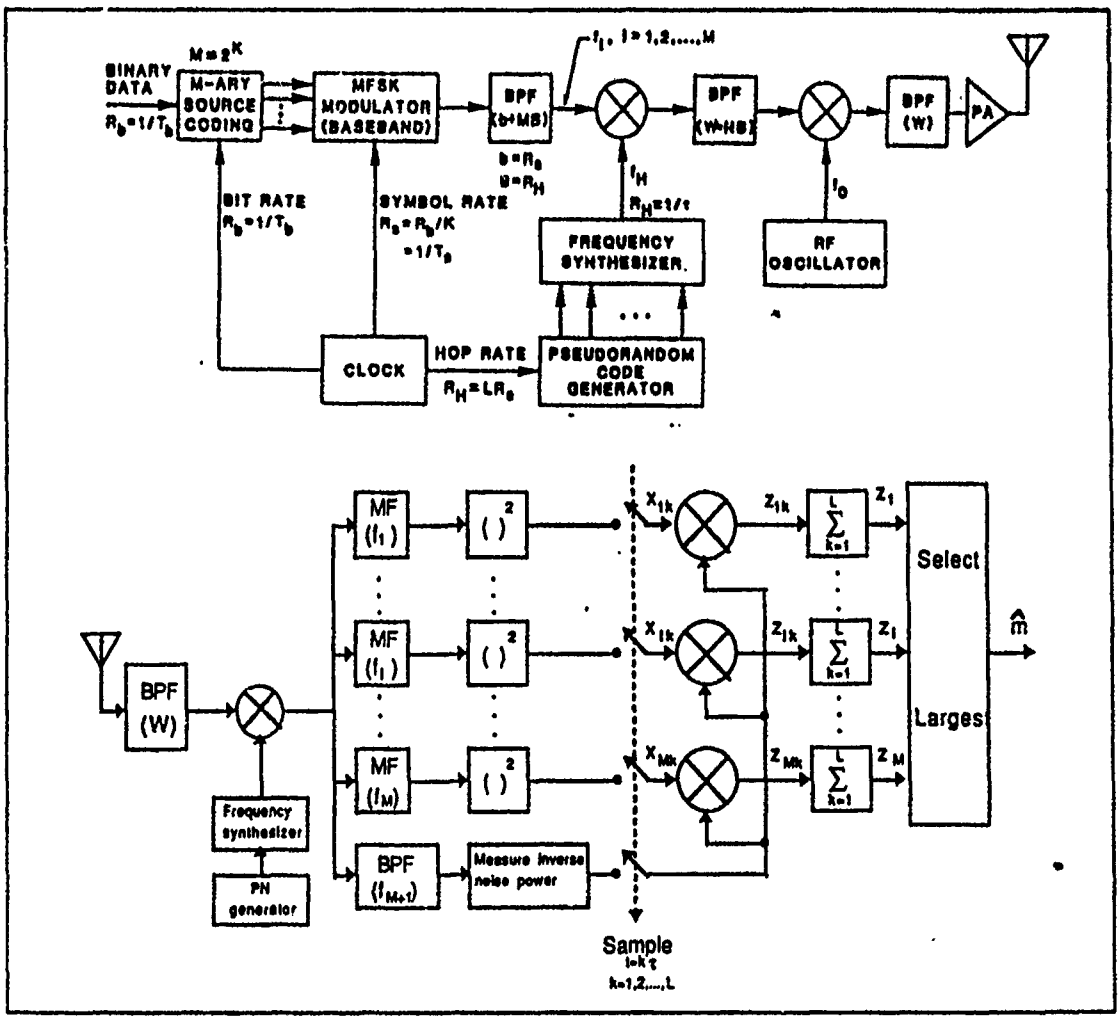

Figure 2. Typical Frequency hopped spread spectrum system

analysis of a proposed fast frequency hopped M-ary frequency shift keyed modulation scheme.

1. Orbit statistics

. Chapter III provides a study of the LASAT orbit distribution and coverage. The first section of the chapter looks into the number of satellites in view of a ground station. An analytical approach was used to derive the mean value and the standard deviation of the number in view. A computer simulation verified the results. The second section of chapter III discusses the coverage of the LASAT relative to a ground terminal. The mean coverage area and the standard

deviation in which connectivity can be established with other ground terminals was found. A computer simulation verified the results.

2. Waveform selection

Waveform selection involves spread spectrum techniques, carrier modulation, error correction coding, and diversity. Chapter IV presents the derivation of the bit error probability for uncoded and coded fast-frequency-hopping M-ary frequency-shift-keying schemes in a Rician fading channel with optimum partial band jamming. Numerical results for various levels of diversity and fading are provided for both the coded and uncoded systems. Convolutional codes and Reed-Solomon codes were used to provide forward error correction coding. Chapter V presents conclusions and recommendations for further research.

III. LASAT SYSTEM

A. DISTRIBUTION OF LASAT

Since the LASAT communication system is envisioned as consisting of a large number of low earth orbiting satellites distributed randomly throughout many orbits, it is expected that the number of satellites in range of a ground station will also be random. The distribution of satellites within view of a ground station will be developed here both theoretically and numerically. The ground station is assumed to have an omnidirectional antenna that will reach satellites with an elevation angle of zero degrees. A general structure of L satellites randomly distributed within an orbit altitude range h_1 to h_2 will be assumed.

1. Theoretical development

The total volume V enclosed by the orbital radii R_1 and R_2 is

$$V = \frac{4}{3}\pi(R_2^3 - R_1^3) \tag{3.1}$$

where

$$\begin{aligned} R_1 &= R_e + h_1 \\ R_2 &= R_e + h_2 \end{aligned} \tag{3.2}$$

with $R_e = 6378.14$ km, (3443.93 NM), the radius of the earth. The volume density of L satellites within this volume is

$$\rho = L/V \quad \text{satellites/km}^3. \tag{3.3}$$

The volume of the orbit portion seen by a ground station can be derived with the help of Figure 3 on page 12. The volume of the spherical sector v_{sec2} defined by points ACBO with radius R_2 is

$$
\begin{aligned}
v_{sec2} &= \int_0^{R_2}\int_0^{2\pi}\int_0^{\alpha} r^2 \sin\theta \, d\theta \, d\phi \, dr \\
&= \frac{2}{3}\pi R_2^3(1-\cos\alpha) \\
&= \frac{2}{3}\pi R_2^2[(R_e+h_2)-R_e] \\
&= \frac{2}{3}\pi R_2^2 h_2
\end{aligned}
\tag{3.4}
$$

where

$$
\cos\alpha = R_e/(R_e+h_2). \tag{3.5}
$$

The right circular cone defined by the points ABO has a volume of

$$
\begin{aligned}
v_{cone} &= \frac{\pi}{3} R_e a^2 \\
&= \frac{\pi}{3}(R_2^2 - R_e^2)R_e.
\end{aligned}
\tag{3.6}
$$

where a is the radius of the base and $a^2 = R_2^2 - R_e^2$. The volume of the segment and base ABC is the difference between the volumes of the spherical sector and the right circular cone.

$$
\begin{aligned}
v_2 &= v_{sec2} - v_{cone} \\
&= \frac{2}{3}\pi(R_e+h_2)^2 - \frac{1}{3}\pi[(R_e+h_2)^2 - R_e^2]R_e \\
&= \frac{1}{3}\pi[2R_e^2h_2 + 4R_eh_2^2 + 2h_2^2 - (R_e^3 + 2R_eh_2 + h_2^2R_e - R_e^3)] \\
&= \frac{1}{3}\pi h_2^2[3R_2 - 3h_2^2 + 2h_2^2] \\
&= \frac{1}{3}\pi h_2^2(3R_2 - h_2).
\end{aligned}
\tag{3.7}
$$

By a similar method, the portion of volume seen by the ground station below h_1 is

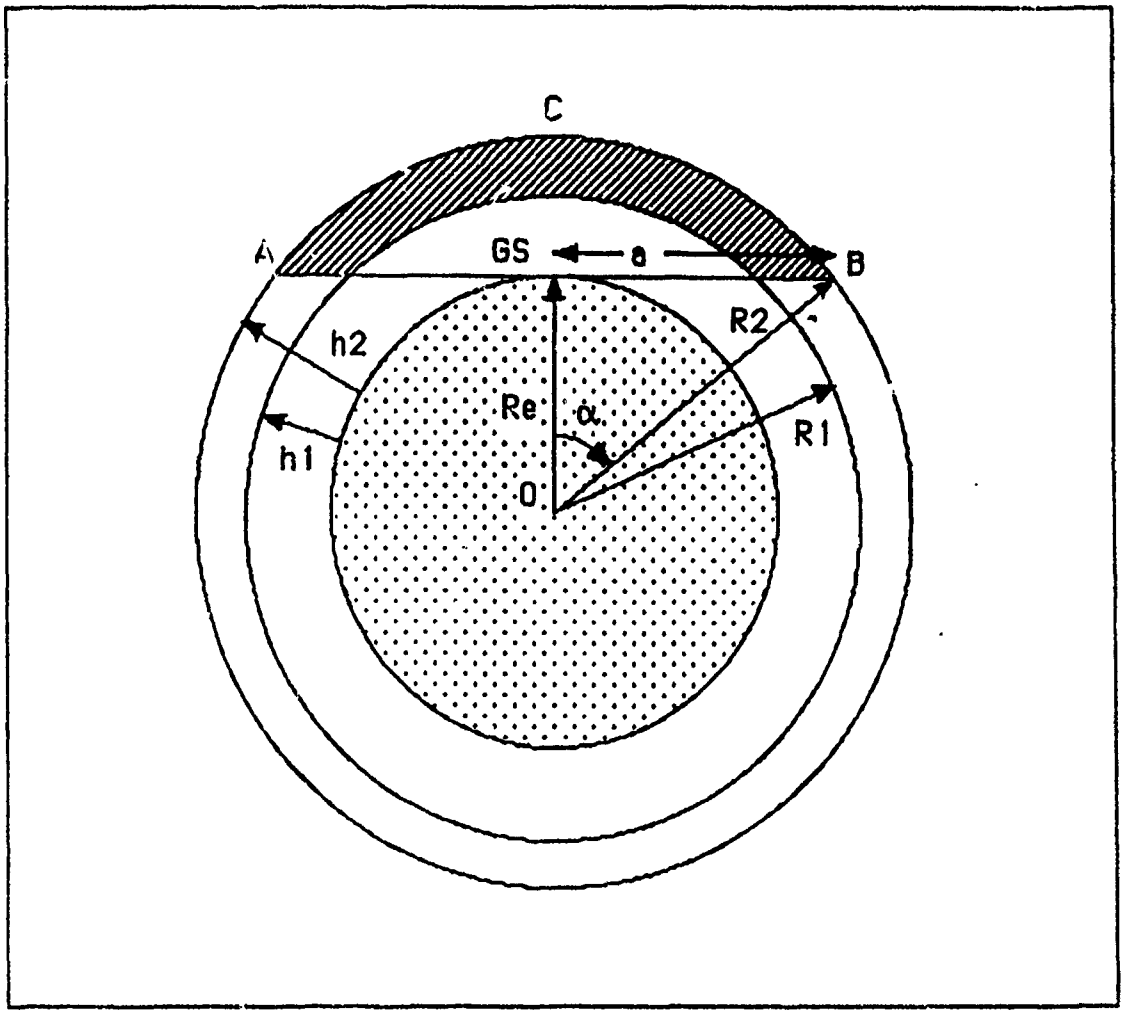

Figure 3. Geometry of satellite orbit distribution.

$$v_1 = \frac{\pi}{3} h_1^2 (3R_1 - h_1), \tag{3.8}$$

and the subvolume v of the orbital shell of thickness $h_2 - h_1$ seen by the ground station is

$$
\begin{aligned}
v &= v_2 - v_1 \\
&= \frac{1}{3}\pi(3h_2^2R_2 - h_2^3) - \frac{1}{3}\pi(3h_1^2R_1 - h_1^3) \\
&= \frac{1}{3}\pi(3h_2^2R_2 - 3h_1^2R_1 - h_2^3 + h_1^3) \\
&= \frac{1}{3}\pi[3h_2^2(R_e + h_2) - 3h_1^2(R_e + h_1) - h_2^3 + h_1^3) \\
&= \frac{1}{3}\pi[3R_e(h_2^2 - h_1^2) + 2h_2^3 - 2h_1^3].
\end{aligned}
\tag{3.9}
$$

Therefore, on average, the number of satellites seen by the ground station will be the density of satellites times the subvolume v, or by using (3.3) and (3.9)

$$
n_{ave} = v\rho = vL/V. \tag{3.10}
$$

The above result can also be shown statistically with the help of the development by Larson [Ref. 6: pp. 143-149]. The distribution of satellites throughout the volume V is random and uniform and one can assume that a volume v can be divided into m non-overlapping subvolumes of size Δv, where $\Delta v = v/m$ is very small. It is therefore reasonable to assume that there will or will not be a satellite in each of these small volumes and that the probability that exactly one satellite will be in each subvolume is $\rho\Delta v = \rho v/m$ for each, where ρ is the density of L satellites distributed throughout the total volume V. Furthermore, it can be assumed that the presence of a satellite in each subvolume is independent of the other subvolumes. Thus the volume v has been subdivided into m repeated independent Bernoulli trials, each of a volume $\Delta v = v/m$ with the probability of a satellite being present equal to $\rho\Delta v = \rho v/m$. If n is the number of satellites in the subvolume v, then n is approximately a binomial random variable with probabiltity density function $f_N(n)$ where

$$
\begin{aligned}
f_N(n) &= \binom{m}{n}\left(\frac{\rho v}{m}\right)^n\left(1 - \frac{\rho v}{m}\right)^{m-n}, \quad n = 0,1,2,\ldots,m \\
&= 0, \quad \text{otherwise.}
\end{aligned}
\tag{3.11}
$$

If the expression is taken to the limit $m \to \infty$ (thus the individual subvolumes are shrinking to zero), the exact probability function for the Poisson random variable results. That is

$$\begin{aligned} f_N(n) &= \lim_{m\to\infty} \binom{m}{n} \left(\frac{\rho v}{m}\right)^n \left(1 - \frac{\rho v}{m}\right)^{m-n} \\ &= \frac{(\rho v)^n}{n!} e^{-\rho v}. \end{aligned} \tag{3.12}$$

Therefore, the distribution of the number of satellites within a volume v can be represented by the volumetric Poisson distribution with a parameter ρv. The well-known mean $\bar{n}$ and variance σ_n^2 of the Poisson process is

$$\bar{n} = \rho v = \frac{Lv}{V}, \tag{3.13}$$

and

$$\sigma_n^2 = \rho v = \frac{Lv}{V}. \tag{3.14}$$

2. Numerical simulation

To generate a sample set representative of the distribution over the orbital volume, a uniform random sequence of L points between 0 and V is generated. To find the number of satellites seen by the ground station for a particular sample set of L points between 0 and V, the number of points between 0 and v are counted, where V and v the orbital volume and subvolume defined by (3.1) and (3.9). When a large number of sample sets are run and the results averaged, the mean number of satellites $\hat{n}$ and the variance $\hat{\sigma}_n^2$ of the samples can be found from

$$\hat{n} = \frac{1}{M} \sum_{i=1}^{M} n_i \tag{3.15}$$

and

$$\hat{\sigma}_n^2 = \frac{1}{M} \sum_{i=1}^{M} (n_i - \hat{n})^2, \tag{3.16}$$

where M is the number of sample sets and n_i is the number of satellites found within the subvolume v in the i th sample set.

Sample means were found by generating first 2000, and then 5000 sample sets of 250 and 150 points uniformily distributed as described above. The number of satellites found in the sub-area were then averaged and compared against the mean found by equation (3.13). Table 1 shows the numerical results for h_1 = 550 km (300 NM) and h_2 = 750 km (400 NM) with 2000 and 5000 samples. The numerical results compare favorably with the theoretical results obtained by (3.15) and (3.16). Differences are due to the pseudo-randomness of the uniform number generator used.

Table 1. MEAN AND VARIANCE OF SATELLITE DISTRIBUTION.

	Theory		2000 Samples		5000 Samples	
L	$\bar{n}$	σ_n^2	$\hat{n}$	$\hat{\sigma}_n^2$	$\hat{n}$	$\hat{\sigma}_n^2$
250	11.54	11.54	12.51	10.43	12.48	10.89
150	6.92	6.92	7.89	6.78	7.87	6.52

When an experiment described by a Poisson process is repeated a great number M of times, then it can be expected that the number M_n of times that exactly n satellites are observed will be [Ref. 7: p. 158]

$$M_n \approx M f_N(n). \tag{3.17}$$

To verify this, the number of satellites found within the subvolume for the run of M = 5000 sample sets was plotted versus the number of times (occurences) M_n that a particular number of satellites were within view (see Figure 4 on page

17). This curve is compared to a Poisson distribution with the parameter ρv as given by (3.13), and shown in Table 1 (see Figure 4 on page 17).

Table 2 shows the maximum number of satellites n_{max} seen by the ground station with a .999 and .990 probability. Since the distribution is Poisson, the probability P that there will be no greater than n_{max} satellites seen by the ground station is

$$P = \Pr[n \leq n_{\max}] = \sum_{n=0}^{n_{\max}} \frac{(\rho v)^n}{n!} e^{-\rho v}. \tag{3.18}$$

The probability P_0 that a ground station sees no satellites overhead is (3.18) with $n_{max} = 0$, or

$$P_0 = e^{-\rho v}, \tag{3.19}$$

and is also given in Table 2

Table 2. NUMBER OF SATELLITES SEEN BY GROUND STATION

L	n_{max} P = 0.999	n_{max} P = 0.99	$n = 0$ P_0
250	22	20	0.00001
150	16	14	0.001

The above analysis shows the expected number of satellites a ground station may communicate with. For a transmitting/receiving pair of ground stations. the number of satellites that may be used for communicating is dependent upon a joint pdf between the number of satellites, the orbital altitude and the distance between the stations. An analysis of the satellite coverage will be covered in the next section.

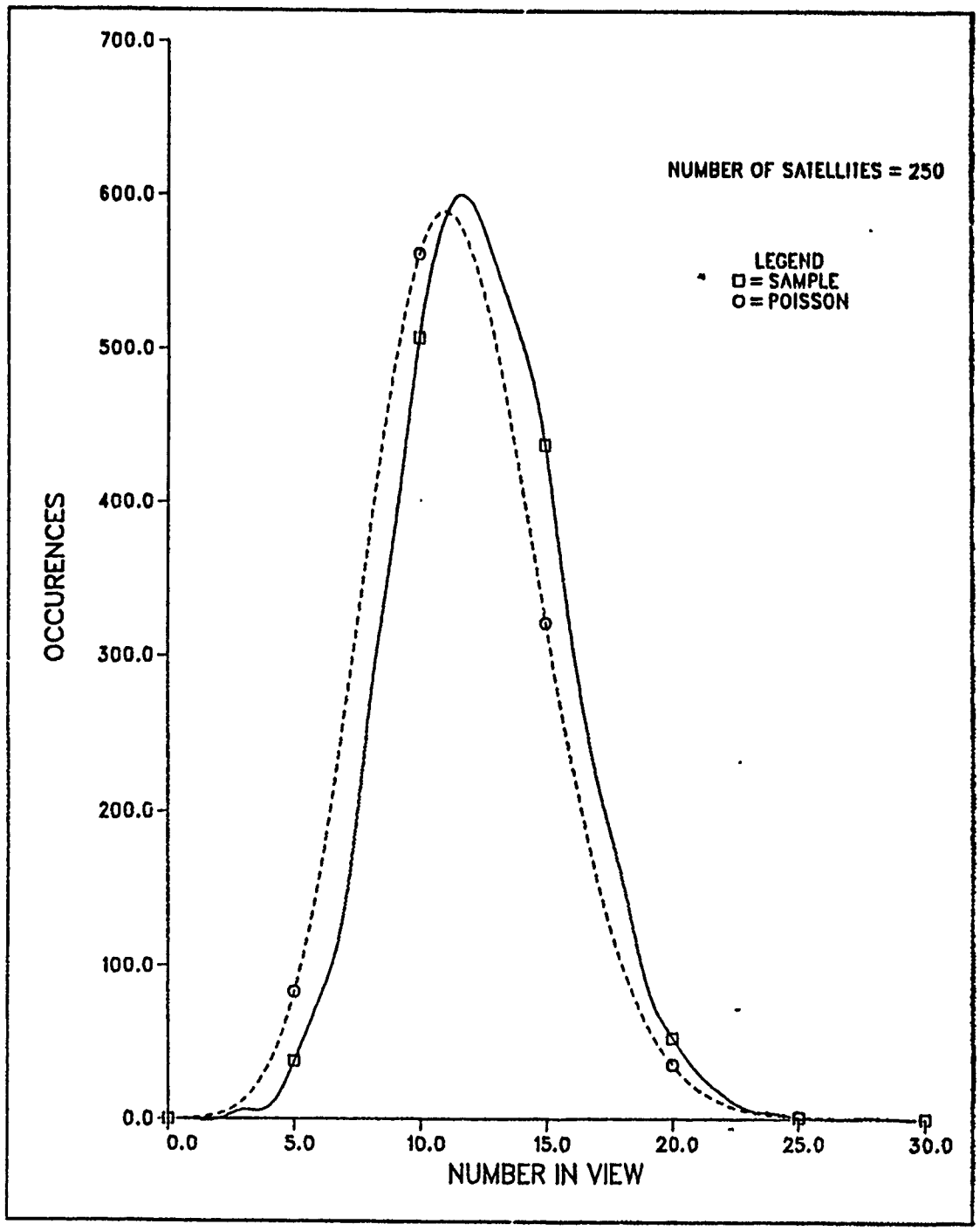

Figure 4. Distribution of the number of satellites within vie Compared with ideal Poisson distribution with parameter $\rho v = 11.54$.

B. COVERAGE

1. Theoretical development

Now that the mean number of satellites seen by a ground station has been established, it is desirable to develope a distribution for the coverage area of the satellites. A satellite on the horizon of the base station has a sub-point that is an angle α away from the base station (see Figure 5 on page 19), where

$$\alpha = \cos^{-1}(R_e/R_2). \tag{3.20}$$

The satellite at point S can communicate an additional distance of arc length $R_e\alpha$ to a user terminal at point UT. Therefore, the base station at point BS has a maximum communication range of arc length $2\alpha R_e$ out to the user terminal through the satellite. This gives a maximum coverage area defined by the solid angle of 4α or $4\cos^{-1}(R_e/R_2)$ steradians, which for an average altitude of $\bar{h} = (h_2 + h_1)/2 = 650$ km (350 NM) is an area of

$$\begin{aligned} A &= R_e^2 \cos^{-1}[R_e/(R_e + \bar{h})] \\ &= 17.63 \times 10^6 \ \text{km}^2. \end{aligned} \tag{3.21}$$

Figure 6 on page 20 shows an example of the coverage area provided by a number of satellites. The spherical caps of area covered by the satellites are shown as circles of an equivelent area. In this diagram there are three satellites, S1, S2, and S3, uniformly spaced over the total view area of the base station (spherical cap of a radius of arc length αR_e from the base station). Each satellite has a range of arc length αR_e also. User terminals, T1, T2, T3, T4, and T5, are also randomly spaced over an area out to a range of arc length $2\alpha R_e$ from the base station. One can see from this Figure 6 that the user terminals have differing numbers of satellites through which they can communicate to the base station. In this example, the user terminals can communicate as follows: T4 through three satellites, T2 through two satellites, T1 and T5 through one satellite each, and T3 has no satellite in range. In general, as the range between the user terminal and the base station increases, there are fewer satellites through which to

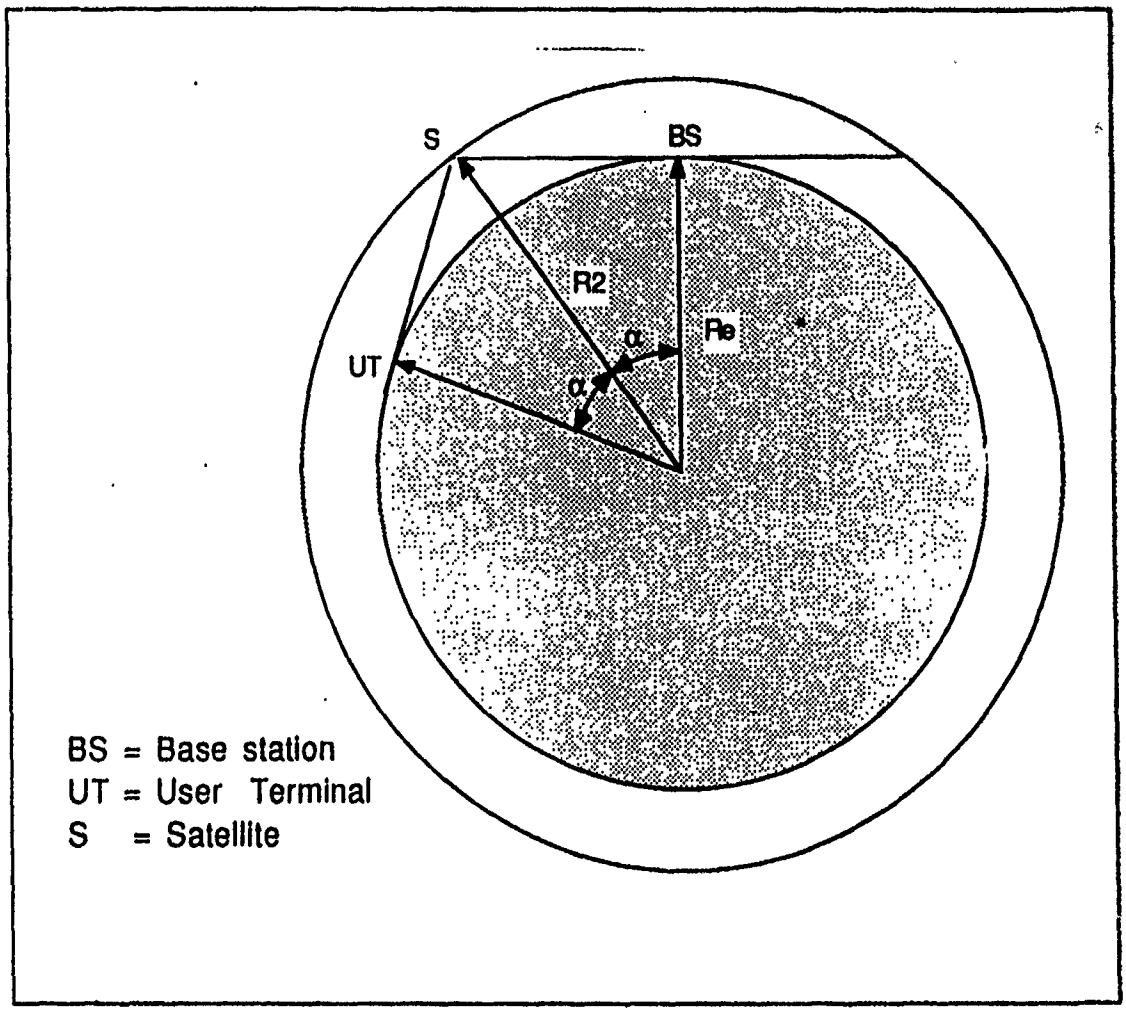

Figure 5. Geometry of satellite coverage.

communicate. If more satellites were added to the system, the communication ablility would increase.

The coverage density for the total number of satellites L in the orbital volume V needs to be determined. This density represents the number of satellites that can communicate with both a user terminal and the base station as a function of the distance r between them for a given number n of satellites that are within view of the base station. The satellites are uniformly distributed through the orbital volume and their different altitudes will result in coverage areas of different sizes. This adds another random variable to the process. Since the

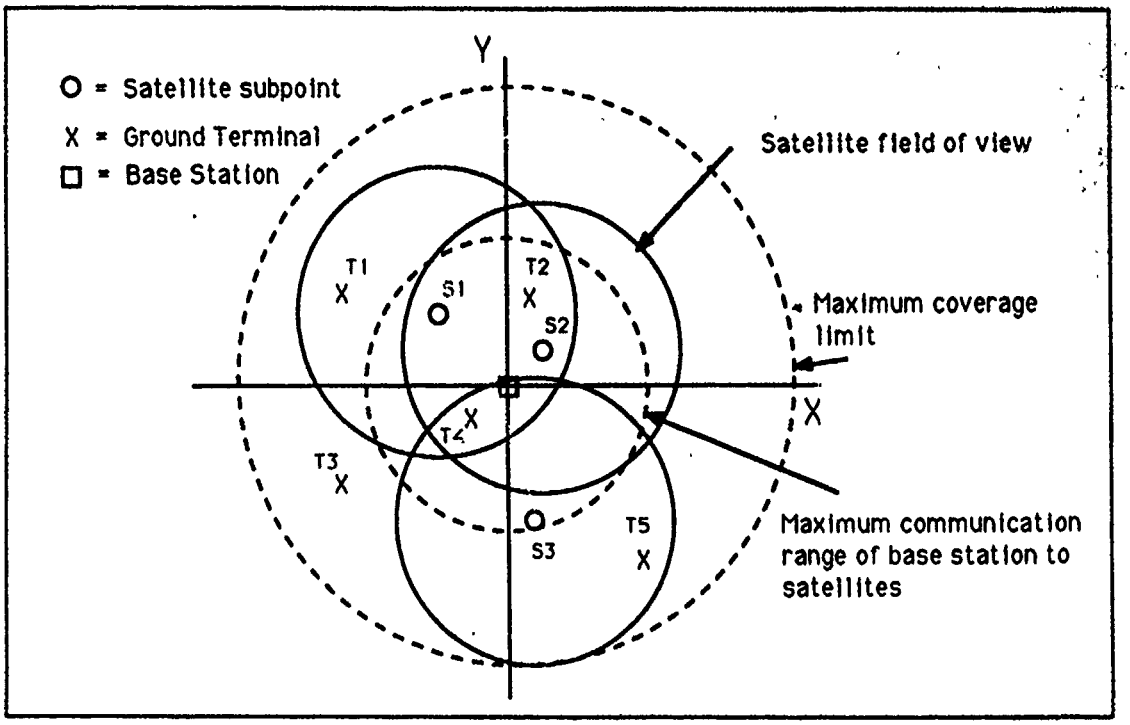

Figure 6. Example of satellite communication range.

altitude difference is assumed to be small compared with the coverage area of each satellite, to simplify calculations without greatly affecting the results, it is safe to assume that all the satellites are at the same altitude and that the orbits are circular. The mean altitude $\bar{h}$ will be used in calculations. The area covered by the satellites can be modeled as an X-Y cartesian grid with the base station at the origin. The positions of the individual satellites are represented by coordinate points x_i and y_i, which are uniformily distributed from $-\alpha R_e$ to αR_e along the X and Y axes. Therefore, the pdfs for the random variables x and y are

$$\begin{aligned} f_X(x) &= 1/2\alpha R_e, \quad -\alpha R_e \le x \le \alpha R_e \\ f_Y(y) &= 1/2\alpha R_e, \quad -\alpha R_e \le y \le \alpha R_e. \end{aligned} \tag{3.22}$$

with a zero mean and a second moment $E[x] = E[y] = \sigma_x^2 = \sigma_y^2 = (\alpha R_e)^2/3$.

For a given number of satellites n, there are n sets of randomly distributed coordinates describing the satellite positions, $x_i, y_i, i = 1,2, \ldots, n$. Each of the satellites covers an area defined by the radius of arc length αR_e around the

satellite subpoint. The average distance from the base station to a satellite subpoint can be described by two new random variables

$$z_x = \frac{1}{n}\sum_{i=1}^{n} x_i$$
$$z_y = \frac{1}{n}\sum_{i=1}^{n} y_i, \tag{3.23}$$

where z_x and z_y are the average X and Y axes coordinates for the satellites. Since n is a Poisson random variable, the distribution of z_x and z_y will be conditioned on n. The conditional probability density functions of z_x and z_y are given by

$$f_{Z_x|N}(z_x|n) = \frac{1}{n}[f_{X_1}(x_1)*f_{X_2}(x_2)* \ldots *f_{X_n}(x_n)]$$
$$f_{Z_y|n}(z_y|n) = \frac{1}{n}[f_{Y_1}(y_1)*f_{Y_2}(y_2)* \ldots *f_{Y_n}(y_n)]. \tag{3.24}$$

where the * is the convolution function. The central limit theory provides that if n is sufficiently large (greater than five), the sum of the random variables approach a Gaussian distribution. Thus, z_x and z_y can be approximated as independent indentically distributed Gaussian random variables with zero mean and a variance of σ_z^2

$$f_{Z_x|n}(z_x|n) = \frac{1}{\sqrt{2\pi\sigma_z^2}}\exp\left\{\frac{-z_x^2}{2\sigma_z^2}\right\}$$
$$f_{Z_y|n}(z_y|n) = \frac{1}{\sqrt{2\pi\sigma_z^2}}\exp\left\{\frac{-z_y^2}{2\sigma_z^2}\right\} \tag{3.25}$$

where

$$\begin{aligned}\sigma_z^2 &= \mathrm{E}[z_x^2] = \mathrm{E}[z_y^2] \\ &= \mathrm{E}\left[\frac{1}{n^2}\sum_{i=1}^{n}\sum_{j=1}^{n}x_i x_j\right] = \frac{1}{n^2}\sum_{i=1}^{n}\sum_{j=1}^{n}\mathrm{E}[x_i x_j] \\ &= \frac{1}{n^2}\sum_{i=1}^{n}E[x_i^2] = \frac{(\alpha R_e)^2}{3n}.\end{aligned} \tag{3.26}$$

Since z_x and z_y are independent, their joint density function is given by

$$\begin{aligned}f_{Z_x Z_y|n}(z_x, z_y|n) &= f_{Z_x|n}(z_x|n) f_{Z_y|n}(z_y|n) \\ &= \frac{1}{2\pi\sigma_z^2}\exp\left\{-\frac{z_x^2 + z_y^2}{2\sigma_z^2}\right\}.\end{aligned} \tag{3.27}$$

The base station can communicate with an area in the shape of a circle with radius $2\alpha R_e$ and the distribution can be represented as a function of the distance r of the user terminal to the base station. To do this, define a new random variable

$$r = \sqrt{z_x^2 + z_y^2}, \tag{3.28}$$

which is the range from the base station to the user terminal, and

$$\begin{aligned}F_{R|n}(r|n) &= \iint_{(z_x, z_y)\in C} f_{Z_x Z_y|n}(z_x, z_y|n)\,dz_x dz_y \\ &= \frac{1}{2\pi\sigma_z^2}\iint_{\sqrt{z_x^2+z_y^2}\le r}\exp\left\{-\frac{z_x^2 + z_y^2}{2\sigma_z^2}\right\}dz_x dz_y.\end{aligned} \tag{3.29}$$

The region C is a circle of radius r. The above integral can be easily solved using polar coordinates [Ref. 8: p. 9]. Let

$$\begin{aligned}z_x &= r\cos\theta \\ z_y &= r\sin\theta \\ dz_x dz_y &= r\,dr\,d\theta,\end{aligned} \tag{3.30}$$

then

$$F_{R|n}(r|n) = \frac{1}{2\pi\sigma_z^2}\int_0^{2\pi}\int_0^{\sqrt{r}} r\exp\left\{-\frac{r^2}{2\sigma_z^2}\right\}drd\theta$$
$$= \left[1-\exp\left\{\frac{-r}{2\sigma_z^2}\right\}\right], \quad r>0, \tag{3.31}$$

and

$$f_{R|n}(r|n) = \frac{d(F_{R|n}(r|n))}{dr} = \frac{1}{2\sigma_z^2}\exp\left\{\frac{-r}{2\sigma_z^2}\right\} \qquad r>0. \tag{3.32}$$

If the substitution for σ_z^2 from (3.24) is made, the result is the exponential density

$$f_{R|n}(r|n) = \frac{3n}{2(\alpha R_e)^2}\exp\left\{\frac{-3rn}{2(\alpha R_e)^2}\right\} \qquad r\geq 0. \tag{3.33}$$

The unconditioned density function $f_R(r)$ can be found by multipling by (3.12) and integrating with respect to n

$$f_R(r) = \int_{-\infty}^{\infty} f_{R|n}(r|n)f_N(n)dn$$
$$= \int_0^{\infty} \frac{3n}{2(\alpha R_e)^2}\exp\left\{\frac{-3rn}{2(\alpha R_e)^2}\right\}\frac{(\rho v)^n}{n!}e^{-\rho v}dn. \tag{3.34}$$

2. Numerical simulation

A numerical simulation of the coverage problem was run to verify the above results. In the model, the average number of satellites that were in view of both a user terminal and the base station were found for various ranges from the base station. This was done by using a sampling raster of points spaced 45 degrees apart on concentric rings around the base station. For each test point, the number of satellites that were within its view range was counted (a satellite was within range if the distance to it from the base station was less than αR_e).

A total was found for all the test points on each ring and the number was divided by the number of test points on the ring (nine) to get the average number of satellites that could be seen from that range.

The sub-satellite points were generated by using a uniform random number generator to provide X and Y axis points that were within a radial distance of one from the base station (the value of αR_e was normalized to one). The set of test points were generated in concentric rings about the origin out to a radius of two. For each test point, the number of sub-satellite points within a radial distance of one were counted (since all sub-satellite points were within a radial distance of one of the base station it was unnecessary to test the base station to satellite distance). The total number of satellites in view for each test ring was then averaged to provide an average number of satellites that can communicate with both the base station and the user terminal for that range.

The test results for three different runs of 13 satellites each are plotted, along with the theoretical result from equation (3.30), in Figure 7 on page 25. The theoretical results were multiplied by the the number of satellites in the array to normalize them with the simulation count. The exponential character of the numerical density is clearly seen and matches very closely to the theoretical results. The difference out near the edge of the range is due to the approximation of the Gaussian function by the central limit theory near the tails of the distribution.

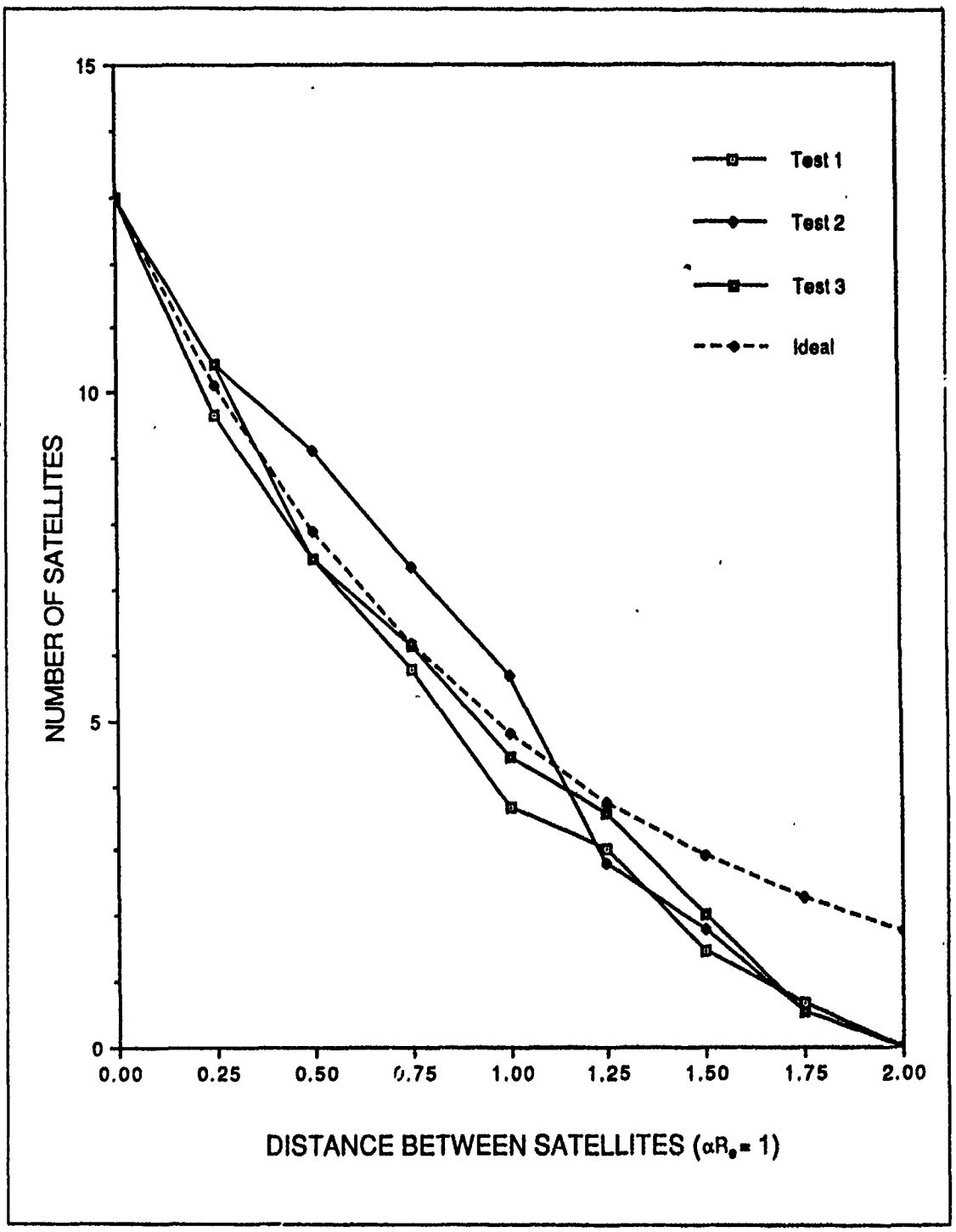

Figure 7. **Coverage density of satellites:** As a function of the distance between terminals.

IV. WAVEFORM ANALYSIS

A. UNCODED FH/MFSK IN A RICIAN FADING CHANNEL WITH PARTIAL BAND JAMMING

The LASAT communications system under consideration must be able to overcome a variety of performance degrading phenomena. Chief among these are: Additive White Gaussian Noise (AWGN), jamming and interference, and fading. Partial band jamming is the optimal jamming strategy most likely to be encountered. Interference may be a result of, among other things, other communications systems, multiple access strategies, or multiple transmitters in the link. For the LASAT communications system the most likely fading encountered will be Rician with a direct line-of-sight component and a random, faded component.

The communications system waveform under consideration in this thesis will be required to overcome the above conditions. The system chosen for study is a fast-frequency-hopped M-ary frequency-shift-keyed (FH/MFSK) system. It is assumed that the channel will be jammed by an intentional jammer whose power resource is AWGN. Channel fading is assumed to be Rician fading with a random faded component due to terrain reflection.

Lindsey [Ref. 9] studied a MFSK system with diversity in a fading channel and showed that diversity is effective in overcomming the effects of fading on the channel. Lee et al. [Ref. 5, 10] considered a special case of the Lindsey system with the diversity applied by fast hopping the MFSK signal. Jamming and coding were applied in the analysis but fading was not. The study done here is a continuation of the work by Lindsey and Lee et al., by considering jamming in a Rician fading channel of a FH/MFSK system.

The transmitter receiver structure similar to Fig. 2 of Ref. 5 is used. A block diagram of the transmitter is shown in Figure 8 on page 28. The binary data is provided at a rate $R_b = 1/T_b$, where T_b is the data bit length, to a M-ary source

coder which provides $M = 2^K$ symbols at a rate $R_s = R_b/K$ Hz. There are L hops per symbol. Each of the symbols is then hopped at a rate $R_h = LR_s$ Hz. Frequency hopping is employed over an allowed system bandwidth W Hz. The carrier is hopped to a new frequency at least once per symbol duration. Thus, the bandwidth of the transmitted radio-frequency pulse is $B = 2/\tau$, where $\tau = T_s/L$, T_s = symbol duration and the bandwidth of the M-ary cluster will be $MB = 2M/\tau$.

The receiver is shown in Figure 9 on page 29. The dehopped signal $r(t)$ is fed into M channels. The output of the square-law detectors are sampled once every $\tau = T_s/L$ seconds to produce the quantities $\{x_{ik}\}$, $i = 1,2,\ldots,M; k = 1,2,\ldots,L$. The detector output samples are multiplied by the weights $1/\sigma_k^2$, which are outputs of a noise only channel estimator, to produce $\{z_{ik}\}$ and are summed over the index k for each i to form the decision statistics $\{z_i\}$. [Ref. 5]

If it is considered that any portion of the system bandwidth W has an equally-likely possibility of being jammed over the jamming bandwidth W/η, where η is the jamming fraction, then a single cell of bandwidth B has a probability η of being jammed and a probability 1- η of not being jammed. Therefore, after dehopping, the received signal in the kth hop can be represented as

$$r_k(t) = \left.\begin{cases} s_k(t) + n_k(t) + j_k(t) & \text{with probability } \eta \\ s_k(t) + n_k(t) & \text{with probability } 1-\eta \end{cases}\right\} \tag{4.1}$$

where $n_k(t)$ and $j_k(t)$ are the independent thermal noise and jamming noise components, respectively.

Without loss of generality it is assumed that the kth hop signal is present at channel 1 and is represented by

$$s_k(t) = a_k \cos(\omega_1 t + \theta_k). \tag{4.2}$$

and has a transmitted energy in the kth hop given by

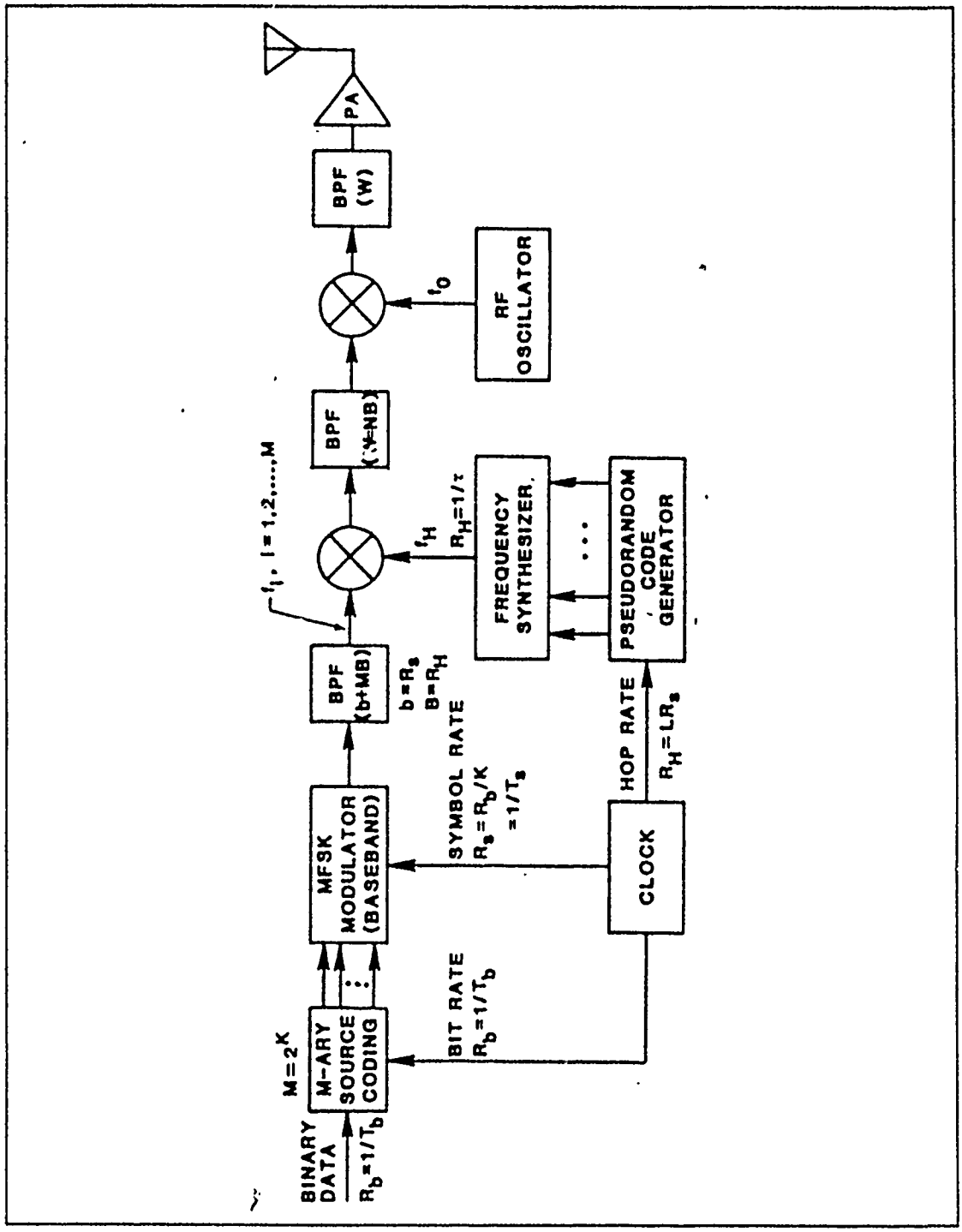

Figure 8. FH/MFSK transmitter: Figure 1 from Ref. 5.

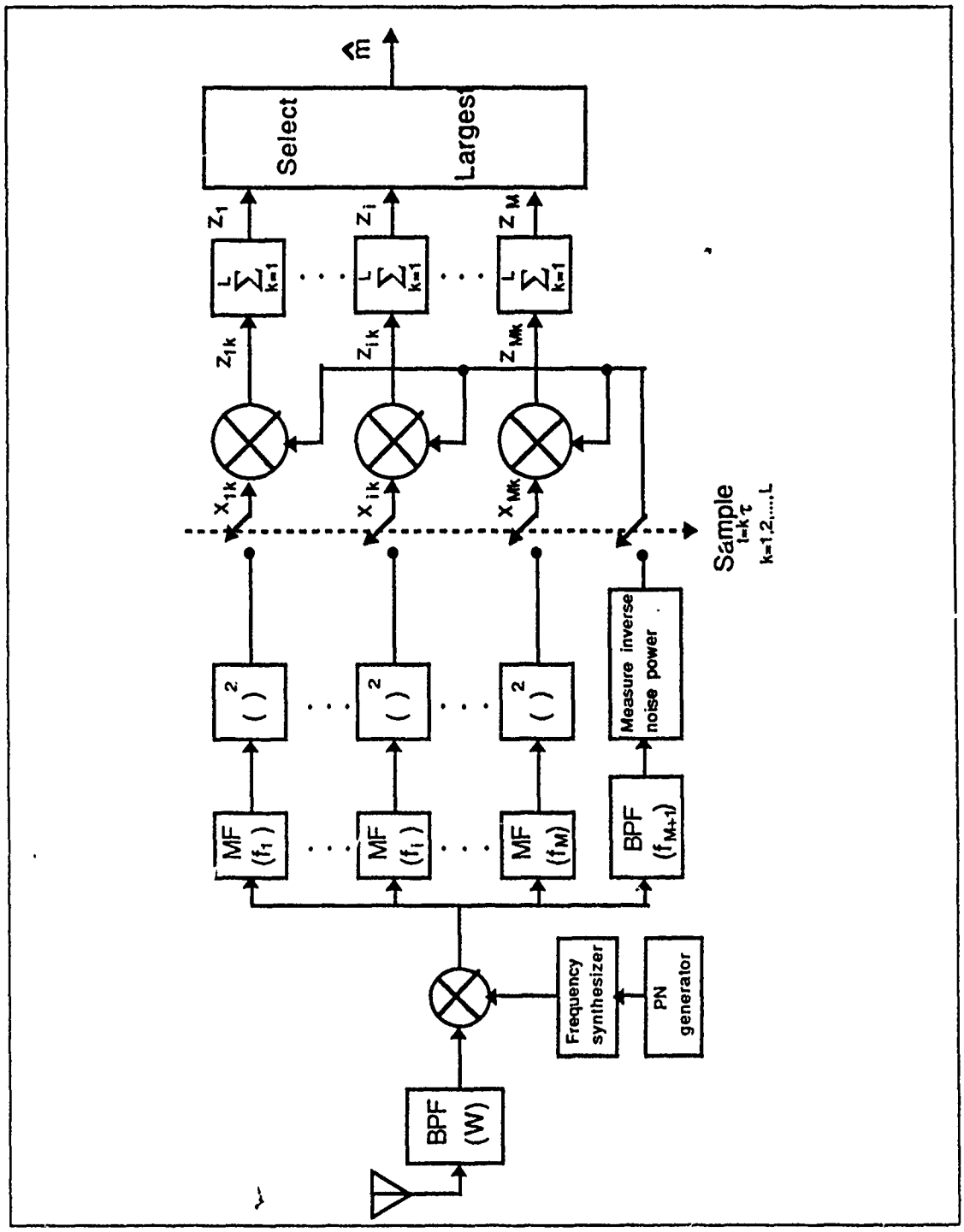

Figure 9. FH/MFSK receiver

$$E_k = E = \frac{1}{2}\int_0^{\tau} \left| \frac{s_k(t)}{a_k} \right|^2 dt, \quad , k = 1,2, \ldots, L, \tag{4.3}$$

where it is assumed that all transmitted signals have equal energy E. The parameter a_k in (4.2) is the Rician variable representing the signal amplitude. The signal $s_k(t)$ has both diffuse and direct (specular) components. Therefore, as discussed in section 2.B the coefficients are Rician distributed and have the density function $f_{A_k}(a_k)$ given by (2.1)

$$f_{A_k}(a_k) = \frac{a_k}{\sigma^2} \exp\left\{ - \frac{a_k^2 + \alpha_k^2}{2\sigma^2} \right\} I_0\left(\frac{a_k \alpha_k}{\sigma^2} \right) \tag{4.4}$$

where

$$I_\alpha(x) = \sum_{p=0}^{\infty} \frac{1}{(p!)(p+\alpha)!} \left(\frac{x}{2} \right)^{2p+\alpha} \tag{4.5}$$

is the modified Bessel function of the first kind of order α. In (4.4), α_k is considered to be the strength of the direct component of $s_k(t)$ and $2\sigma^2$ is the mean-squared value of the diffuse component in $s_k(t)$. For convenience define $\gamma_k^2 = \alpha_k^2/2\sigma^2$ as the direct-to-diffuse power ratio of $s_k(t)$. If γ_k^2 approaches zero (absence of direct components). the density $f_{A_k}(a_k)$ represents Rayleigh fading, while if γ_k^2 approaches infinity (presence of direct components) the density function represents a Gaussian channel with mean α_k. [Ref. 9]

Thermal noise is assumed to be present in each channel and is additive white Gaussian noise (AWGN) with zero mean and a variance of $\sigma_\chi^2 = N_0 B$, where N_0 is the one-sided (AWGN) power spectral density and B is the channel bandwidth. The noise is assumed to be statistically independent and identically distributed in each channel. For no jamming, the received kth hop signal may be represented as

$$r_k(t) = a_k \cos(\omega_1 t + \theta_k) + n_k(t), \quad k = 1,2 \ldots ,L. \tag{4.6}$$

The signal can be expanded into in-phase and quadrature components which gives

$$\begin{aligned} r_k(t) &= a_k(\cos \omega_1 t \cos \theta_k - \sin \omega_1 t \sin \theta_k) + n_{ck}(t) \cos \omega_1 t - n_{sk}(t) \sin \omega_1 t \\ &= [a_k \cos \theta_k + n_{ck}(t)] \cos \omega_1 t - [a_k \sin \theta_k + n_{sk}(t)] \sin \omega_1 t \\ &= x_{ck}(t) \cos \omega_1 t - x_{sk}(t) \sin \omega_1 t, \end{aligned} \tag{4.7}$$

where $n_{ck}(t)$, and $n_{sk}(t)$ are the independent noise quadrature components in all channels. The output samples of the square-law detectors on the kth hop are, dropping the time dependence, for the signal channel

$$\begin{aligned} x_{1k} &= x_{ck}^2 + x_{sk}^2 \\ &= (a_k \cos \theta_k + n_{ck})^2 + (a_k \sin \theta_k + n_{sk})^2, \end{aligned} \tag{4.8}$$

and for the other channels

$$x_{ik} = n_{ck}^2 + n_{sk}^2, \quad i = 2,3, \ldots ,M. \tag{4.9}$$

When jamming occurs, it is considered to be present in all M channels and the measurement channel. The jammer is assumed to spread its total available power J uniformly over the fraction η of the bandwidth W. $0 < \eta \leq 1$. The average jamming spectral density is $N_J = J/W$ Watts/Hz. The jamming spectral density over the actual jammed fraction of the band is N_J/η Watts. The combination of jamming and thermal noise on the kth hop produces the detector output samples for the signal channel

$$x_{1k} = (a_k \sin \theta_k + n_{ck} + j_{ck})^2 + (a_k \cos \theta_k + n_{sk} + j_{sk})^2, \tag{4.10}$$

and for the other channels

$$x_{ik} = (n_{ck} + j_{ck})^2 + (n_{sk} + j_{sk})^2, \quad i = 2,3, \ldots , M, \tag{4.11}$$

where j_{ck}, and $j_{sk}, k = 1,2,\ldots,L$ are the independent jamming noise quadrature components in all channels and are assumed to be additive Gaussian noise with variance defined by $\sigma_j^2 = N_J B/\eta$.

Following the derivation by Lee et al. [Ref. 5], the error probability expression can be derived. If equally likely M-ary symbols are assumed, the expression for the symbol error probability, given signal of channel 1 is sent, is

$$P_s(e) = \sum_{l=0}^{L} P_l P_s(e \mid l \text{ hops jammed}) \tag{4.12}$$

where

$$P_l = \binom{L}{l} \eta^l (1-\eta)^{L-l} \tag{4.13}$$

is the probability that l out of L channels are jammed, and

$$P_s(e \mid l) = 1 - P_s(c \mid l) \tag{4.14}$$

is the probability that an error was made given l channels are jammed. $P_s(c \mid l)$ is the probability of a correct decision given that signal of channel 1 is sent and l hops are jammed.

Whalen [Ref. 4: sec 4.7, 4.8.] shows that the square-law detector output has a probability density function which is noncentral chi-squared; thus, for a given amplitude a_k,

$$f_{X_{1k}}(x_{1k} \mid a_k) = \frac{1}{2\sigma_k^2} \exp\left\{ -\frac{x_{1k} + a_k^2}{2\sigma_k^2} \right\} I_0\left[\frac{(x_{1k})^{1/2} a_k}{\sigma_k^2} \right], \tag{4.15}$$

where $\sigma_k^2 = NB = 2N/\tau = 2NL/T_s$. The total noise density N is given by

$$N = \begin{cases} N_0 & \text{with probability } 1-\eta \\ N_T = (N_0 + N_J/\eta) & \text{with probabilty } \eta. \end{cases} \tag{4.16}$$

The output of the detector is then normalized by dividing by the output of the channel estimator which results in the variable $z_{ik} = x_{ik}/\sigma_k^2$, $i = 1,2, \ldots, M$, which has a conditional pdf, for the signal channel,

$$f_{Z_{1k}}(z_{1k} \mid a_k) = \frac{1}{2} \exp\left\{ -\frac{z_{1k}}{2} - \frac{a_k^2}{2\sigma_k^2} \right\} I_0\left[\frac{(z_{1k})^{1/2} a_k}{\sigma_k} \right]. \tag{4.17}$$

The unconditional probability density function for z_{1k} can be found by integrating (4.17) over all a_k

$$f_{Z_{1k}}(z_{1k}) = \int_0^\infty f_{Z_{1k} \mid A_k}(z_{1k} \mid a_k) f_{A_k}(a_k) da_k, \tag{4.18}$$

or (see Appendix),

$$f_{Z_{1k}}(z_{1k}) = \frac{1}{2(1+\beta)} \exp\left\{ -\frac{z_{1k} + 2\rho_k}{2(1+\beta)} \right\} I_0\left(\sqrt{\frac{z_{1k} 2\rho_k}{(1+\beta)^2}} \right), \tag{4.19}$$

where $\beta = 2\sigma^2 R$ is the output signal-to-noise ratio produced by the diffuse component, and $\rho_k = \alpha_k^2 R$ is the output signal-to-noise ratio of the specular (direct) component of the k th hop signal in channel 1. The ratio R is defined as

$$\begin{aligned} R &= \frac{E}{N} = \frac{\text{hop energy of transmitted signal}}{\text{total noise density}} \\ &= \frac{\tau}{4N} = \frac{1}{2BN} = \frac{1}{2\sigma_k^2}. \end{aligned} \tag{4.20}$$

The decision statistics at the output of the summers are

$$z_i = \sum_{k=1}^{L} z_{ik}, \qquad i = 1,2, \ldots, M. \tag{4.21}$$

The probability density function for z_i may be found using characteristic functions. With the use of the tables of Fourier transforms by Campbell and Foster

(pair 655.1) [Ref. 11: p. 79] the characteristic function of $f_{Z_{1k}}(z_{1k})$ in (4.19) is given by

$$\Phi_{Z_{1k}}(p) = \frac{1}{2(1+\beta)} \exp\left\{ \frac{-2\rho_k}{2(1+\beta)} \right\} \frac{1}{p+\psi} \exp\left\{ \frac{1}{\xi_k(p+\psi)} \right\}, \quad (4.22)$$

where p is the complex variable and

$$\psi = \frac{1}{2}(1+\beta) \text{ and } \xi_k = \frac{4(1+\beta)^2}{2\rho_k}. \quad (4.23)$$

Since the z_{1k}'s are independent and identically distributed, the characteristic function of the decision statistic z_1 can be found from

$$\Phi_{Z_1}(p) = \prod_{k=1}^{L} \Phi_{Z_{1k}}(p). \quad (4.24)$$

Combining (4.22) and (4.24) yields

$$\Phi_{Z_1}(p) = \frac{1}{[2(1+\beta)]^L} \exp\left\{ \frac{-\sum_{k=1}^{L} 2\rho_k}{2(1+\beta)} \right\} \cdot \frac{1}{(p+\psi)^L} \exp\left\{ \frac{1}{\sum_{k=1}^{L} \xi_k (p+\psi)} \right\}. \quad (4.25)$$

From Ref. 11: pair 650, p. 77, the probability density function for z_1 is obtained as follows:

$$f_{Z_1}(z_1) = \frac{1}{2(1+\beta)} \left(\frac{z_1}{2\rho_l} \right)^{\frac{L-1}{2}} \exp\left\{ -\frac{z_1 + 2\rho_l}{2(1+\beta)} \right\} \cdot I_{L-1}\left[\sqrt{\frac{z_1 2\rho_l}{(1+\beta)^2}} \right], \quad (4.26)$$

$z_1 > 0$. The noncentral parameter of (4.26) is

$$\rho_l = \sum_{k=1}^{L} \rho_k = \sum_{k=1}^{L} \alpha_k^2 R = 2\sigma^2 R \sum_{k=1}^{L} \gamma_k^2, \tag{4.27}$$

where $\gamma_k^2 = \alpha_k^2/2\sigma^2$ is the direct-to-diffuse power ratio and

$$R = \frac{E}{N} = \frac{E_s}{NL} = \frac{KE_b}{NL} \tag{4.28}$$

is the energy per hop to noise density ratio, with E_s as the symbol energy, and E_b as the bit energy. Then, if it is assumed that l out of L channels are jammed,

$$\begin{aligned} \rho_l &= 2\sigma^2 \frac{E}{N} \sum_{k=1}^{L} \gamma_k^2 \\ &= 2\sigma^2 \sum_{k=1}^{L} \gamma_k^2 \left(\frac{l}{L} \frac{KE_b}{LN_T} + \frac{(L-l)}{L} \frac{KE_b}{LN_0} \right) \\ &= 2\sigma^2 \frac{K}{L} \bar{\gamma}^2 \left[l \frac{E_b}{N_T} + (L-l) \frac{E_b}{N_0} \right], \end{aligned} \tag{4.29}$$

where

$$\bar{\gamma}^2 = \frac{1}{L} \sum_{k=1}^{L} \gamma_k^2 \tag{4.30}$$

is the mean direct-to-diffuse power ratio with N_0 and N_T are from (4.16).

With the use of the definition of the Bessel function (4.5), equation (4.26) can be expressed as

$$f_{Z_1}(z_1) = \frac{e^{-\rho_l/(1+\beta)}}{2(1+\beta)} \sum_{p=0}^{\infty} \frac{(\rho_l/1+\beta)^p}{p!\Gamma(p+L)} \exp\left\{ \frac{-z_1}{2(1+\beta)} \right\} \left(\frac{z_1}{2(1+\beta)} \right)^{p+L-1}. \quad (4.31)$$

As in the non-fading case with a fixed amplitude, the pdf for the noise only channels, z_i, $i = 2,3, \ldots, M$, is chi-squared with $2L$ degrees of freedom and may be obtained from (4.32) with $\rho_l = 0$, $z_1 = z_i$, and $\beta = 0$

$$f_{Z_i}(z_i) = \frac{(z_i/2)^{L-1}}{2\Gamma(L)} \exp(-z_i/2), \qquad z_i > 0, \quad i = 2,3, \ldots, M. \quad (4.32)$$

Equation (4.14) can then be found from

$$P_s(e \mid l) = 1 - \int_0^{\infty} f_{Z_1}(z_1) \left[\int_0^{z_1} f_{Z_i}(z_i) dz_i \right]^{M-1} dz_1. \quad (4.33)$$

Substituting the appropriate distributions (4.31) and (4.32) into (4.33) above yields

$$P_s(e \mid l) = 1 - \int_0^{\infty} \frac{e^{-\frac{\rho_l}{1+\beta}}}{2(1+\beta)} \sum_{p=0}^{\infty} \frac{(\rho_l/2(1+\beta))^p}{p!\Gamma(p+L)} \exp\left\{ \frac{-z_1}{2(1+\beta)} \right\} \left(\frac{z_1}{2(1+\beta)} \right)^{p+L-1} \cdot \left[\frac{1}{2\Gamma(L)} \int_0^{z_1} \left(\frac{z_i}{2} \right)^{L-1} e^{-z_i/2} dz_i \right]^{M-1} dz_1. \quad (4.34)$$

The solution to the integral inside the brackets is

$$\left[\int_0^{z_1} f_{Z_i}(z_i) dz_i \right]^{M-1} = \left[1 - e^{-z_1/2} \sum_{r=0}^{L-1} \frac{(z_1/2)^r}{r!} \right]^{M-1}, \quad (4.35)$$

which can be expanded to

$$= \sum_{m=0}^{M-1} \binom{M-1}{m} (-1)^m \left[e^{-z_1/2} \sum_{r=0}^{L-1} \frac{(z_1/2)^r}{r!} \right]^m \tag{4.36}$$

$$= \sum_{m=0}^{M-1} \binom{M-1}{m} (-1)^m e^{-mz_1/2} \sum_{r=0}^{mL-m} \frac{C_r(m,L)}{r!} \left(\frac{z_1}{2} \right)^r, \tag{4.37}$$

where

$$C_r(m,L) = \frac{1}{r} \sum_{n=1}^{W} \binom{r}{n} [(n+1)n - r] C_{r-n}(m,L) \tag{4.38}$$

with

$$W = \begin{Bmatrix} r & \text{for} \quad 0 \le r \le L-1 \\ L-1 & \text{for} \quad r > L-1 \end{Bmatrix}. \tag{4.39}$$

Equation (4.38) is a modified version of the J. P. Miller formula [Ref. 12 : p. 42] for the coefficients of a composition of a formal power series and a nonunit. Composition is the substitution of one power series into another. The Miller formula applies when one series is a binomial series. Substituting (4.37) into (4.34) gives

$$P_s(e\,|\,l) = 1 - \left[\frac{e^{-\frac{\rho_l}{1+\beta}}}{1+\beta} \sum_{p=0}^{\infty} \frac{(\rho_l/1+\beta)^p}{p!\Gamma(p+L)} \right]$$
$$\cdot \sum_{m=0}^{M-1} \binom{M-1}{m} (-1)^m \sum_{r=0}^{mL-m} \frac{C_r(m,L)}{r!} \tag{4.40}$$
$$\cdot \left[\frac{(1+\beta)^r}{2} \int_0^{\infty} \exp\left\{ - \frac{[m(1+\beta)+1]z_1}{2(1+\beta)} \right\} \left(\frac{z_1}{2(1+\beta)} \right)^{p+L+r-1} dz_1 \right].$$

It can be shown that [Ref. 13: p. 438]

$$1 - \sum_{m=0}^{M-1} \binom{M-1}{m} (-1)^m \sum_{r=0}^{mL-m} \frac{C_r(m,L)}{r!} (X)^r$$
$$= \sum_{m=1}^{M-1} \binom{M-1}{m} (-1)^{m+1} \sum_{r=0}^{mL-m} \frac{C_r(m,L)}{r!} (X)^r. \tag{4.41}$$

Solving the integral and and using (4.41), yields

$$P_s(e\,|\,l) = \sum_{m=1}^{M-1} \binom{M-1}{m} \frac{(-1)^{m+1}}{(1+m+m\beta)^L} \exp\left\{ \frac{-\rho_l}{1+\beta} \right\}$$
$$\cdot \sum_{r=0}^{mL-m} \frac{C_r(m,L)}{r!} \left[\frac{1+\beta}{1+m+m\beta} \right]^r \tag{4.42}$$
$$\cdot \sum_{p=0}^{\infty} \frac{(\rho_l)^p}{p!\Gamma(p+L)} \frac{(p+r+L-1)!}{(1+\beta)^p(1+m+m\beta)^p}.$$

With some rearanging (4.42) can be written as

$$P_s(e|l) = \sum_{m=1}^{M-1} \binom{M-1}{m} \frac{(-1)^{m+1}}{(1+m+m\beta)^L} \exp\left\{ \frac{-\rho_l}{1+\beta} \right\}$$
$$\cdot \sum_{r=0}^{mL-m} C_r(m,L) \left[\frac{1+\beta}{1+m+m\beta} \right]^r \frac{(r+L-1)!}{r!(L-1)!} \qquad (4.43)$$
$$\cdot \left[\sum_{p=0}^{\infty} \frac{(\rho_l)^p}{p!(1+\beta)^p(1+m+m\beta)^p} \frac{(r+L)_p}{(L)_p} \right].$$

The portion in the brackets is equal to the confluent hypergeometric series ${}_1F_1(r+L; L; w)$ [Ref. 12: Vol II, p. 260, Ref. 14: p. 1250] and is given by[1]

$${}_1F_1(r+L; L; w) = \frac{L_r^{(L-1)}(-w)e^w}{\binom{r+L-1}{r}} = e^w {}_1F_1(-r; L; -w) \qquad (4.47)$$

where

$$w = \frac{\rho_l}{1+\beta(1+m+m\beta)}. \qquad (4.48)$$

---

1 Details on the derivation of equation (4.47).

$${}_1F_1(r+L; L; w) = \sum_{p=0}^{\infty} \frac{(L+1)_p}{(L)_p} \frac{w^p}{p!} = \sum_{p=0}^{\infty} \frac{\Gamma(L+r+p)}{\Gamma(L+r)} \frac{\Gamma(L)}{\Gamma(L+p)} \frac{\tau^p}{p!} \qquad (4.44)$$

$$= \sum_{p=0}^{\infty} \frac{(L+r+p-1)!}{(L+p-1)!} \frac{\tau^p}{(p!)} \frac{(L-1)!\,(r!)}{(L+r-1)!\,(r!)} = \frac{e^w}{r!} L_r^{(L-1)}(w) / \binom{r+L-1}{r}. \qquad (4.45)$$

where

$${}_1F_1(a; b; w) = \sum_{p=0}^{\infty} \frac{(a)_p}{(b)_p} \frac{w^p}{p!}, \qquad (a)_p = \frac{\Gamma(a+p)}{\Gamma(a)} \qquad (4.46)$$

$L_n^m(w)$ is the generalized Laguerre polynomial, which in this case equals

$$L_r^{(L-1)}(-w) = \sum_{p=0}^{r} \frac{(-1)^p}{p!} \binom{r+L-1}{r-p} (-w)^p$$
$$= \frac{(L)_r}{r!} {}_1F_1(-r;L;-w). \tag{4.49}$$

Substituting (4.47) into (4.43) gives the desired result

$$P_s(e|l) = \sum_{m=1}^{M-1} \binom{M-1}{m} \frac{(-1)^{m+1}}{(1+m+m\beta)^L} \exp\left\{ \frac{-m\rho_l}{1+m+m\beta} \right\}$$
$$\cdot \sum_{r=0}^{mL-m} C_r(m,L) \left[\frac{1+\beta}{1+m+m\beta} \right] \tag{4.50}$$
$$\cdot \sum_{p=0}^{r} \frac{(\rho_l)^p}{p!(1+\beta)^p(1+m+m\beta)^p} \binom{p+L-1}{p-r}.$$

The result from Lindsey [(41), Ref. 9] for the symbol error can be obtained from (4.50) by letting $\eta = 0$, the no-jamming case, and using the hypergeometric series definition (4.47)

$$P_s(e) = \sum_{m=1}^{M-1} \binom{M-1}{m} \frac{(-1)^{m+1}}{(1+m+m\beta)^L} \exp\left\{ \frac{-m\rho_0}{1+m+m\beta} \right\}$$
$$\cdot \sum_{r=0}^{mL-m} \frac{C_r(m,L)}{r!} \frac{\Gamma(L+r)}{\Gamma(L)} \left[\frac{1+\beta}{1+m+m\beta} \right]^r \tag{4.51}$$
$$\cdot {}_1F_1\left[-r; L; \frac{-\rho_0}{(1+\beta)(1+m+m\beta)} \right]$$

where ρ_0 is (4.30) with $l = 0$.

Bit error probability from symbol error for an M-ary orthogonal system (MFSK) is given by

$$P_b(e) = \frac{M}{2(M-1)} P_s(e) \tag{4.52}$$

where the probability of symbol error is given by equation (4.12). Using (4.13), (4.50), and (4.52) in (4.12) gives the probability of bit error for the receiver

$$P_b(e) = \frac{M}{2(M-1)} \sum_{l=0}^{L} \binom{L}{l} \eta^l (1-\eta)^{L-l} \sum_{m=1}^{M-1} \binom{M-1}{m} \frac{(-1)^{m+1}}{(1+m+m\beta)^L} \exp\left\{ \frac{-m\rho_l}{1+m+m\beta} \right\} \sum_{r=0}^{mL-m} C_r(m,L) \left[\frac{1+\beta}{1+m+m\beta} \right]^r \cdot \sum_{p=0}^{r} \frac{(\rho_l)^p}{p!(1+\beta)^p (1+m+m\beta)^p} \binom{p+L-1}{p-r}. \tag{4.53}$$

For the non-fading case, $2\sigma^2 = 0$ and $\alpha_k = 1$ for all k, and if the definition for the Laguerre polynomial (4.49) is used the result is equation (16) from Ref. 5

$$P_s(e|l) = \sum_{m=1}^{M-1} \binom{M-1}{m} \frac{(-1)^{m+1}}{(m+1)^L} \exp\left(\frac{-m}{m+1} \rho_l \right) \cdot \sum_{r=0}^{mL-m} \frac{C_r(m,L)}{(m+1)^r} L_r^{(L-1)}\left(-\frac{\rho_l}{m+1} \right). \tag{4.54}$$

B. CODED FH/MFSK IN A RICIAN FADING CHANNEL WITH PARTIAL BAND JAMMING

The diversity studied in the last section is an effective means of overcoming the detrimental effects of fading. Frequency diversity, however, is a trivial form of repetitive coding and the decision statistic of the receiver is soft decision decoding of the repetitive code. More complex types of codes may also be used to provide diversity which is much more efficient than frequency diversity [Ref. 3: p. 753].

Forward Error Correction (FEC) codes can be used to provide improved performance with fading signals without having to use large amounts of diversity which cause increases in the recombining losses caused by the summing operations. To apply coding, the circuit of Figure 8 on page 28 is modified with the addition of a binary to Q-ary encoder and a Q-ary to binary decoder as shown in Figure 10 on page 43. Information bits from a binary source at a rate R_b are mapped to Q-ary symbols where $Q = 2^q$ at a rate $R_q = R_b/q$ and applied to the coder input. The forward error correction coder outputs n Q-ary symbols for every k Q-ary input symbols. This gives a code rate $r = k/n$ and the coder output rate is $R_c = nR_q/k = nR_b/kq$. The channel modulation is FH/MFSK with $M = 2^K$. The modulator input rate is $R_d = qR_c/K = nR_b/kK$. The M-ary words are applied to a MFSK modulator which selects one of M baseband frequencies, f_i, $i = 1,2, \ldots, M$. The modulator output symbols are then hopped at a rate of L hops per symbol, or $R_h = LR_d = nLR_b/kK$. The bandwidth of the transmitted pulse is $B = 2/\tau$, where $\tau = T_d/L$, T_d = symbol rate. The total system bandwidth is made-up of N_h possible frequencies spaced B Hz apart so that $W = N_h B$ Hz. [Ref. 10]

The receiver block diagram is also shown in Figure 10 on page 43. The demodulator operation is the same as described in section 4.A. After a decision is made as to which channel has the largest output, the M-ary words are converted into Q-ary symbols and sent to the decoder input. The decoder makes a hard decision as to what Q-ary symbol was sent. A Q-ary to binary converter then reconstructs the binary series $\{\hat{X}\}$.

If the transmitted energy per information bit is defined by (4.28), then the energy per coded M-ary word is

$$E_d = \frac{kKE_b}{n} \tag{4.55}$$

and the energy per hop is

$$E_h = \frac{E_d}{n} = \frac{kKE_b}{nL} \tag{4.56}$$

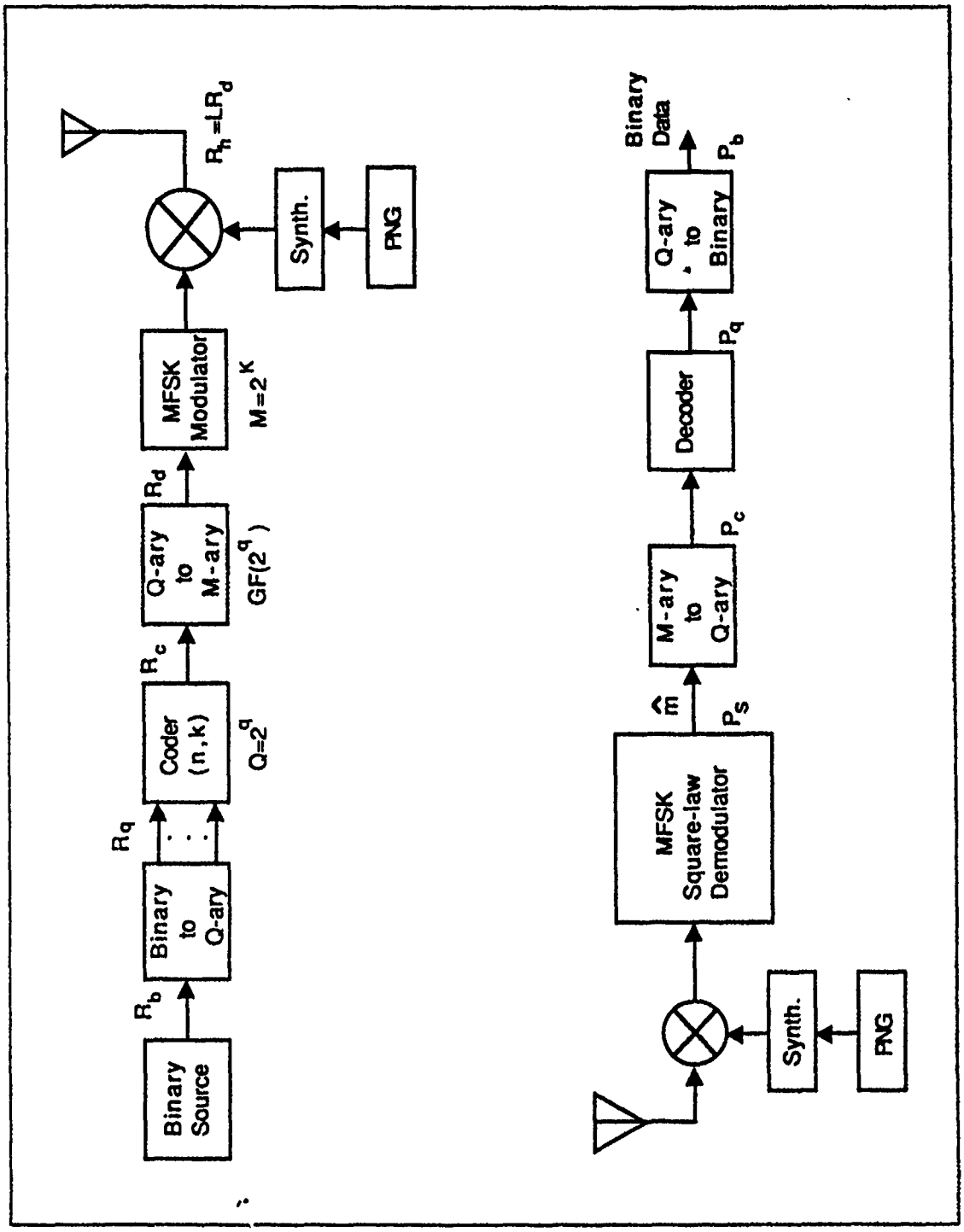

Figure 10. FH/MFSK system with coding: Figure 1 from Ref. 10.

The probability of word error at the output of the decision maker is the same as without coding, namely

$$P_s(e) = \sum_{l=0}^{L} \binom{L}{l} \eta^l (1-\eta)^{L-l} \sum_{m=1}^{M-1} \binom{M-1}{m} \frac{(-1)^{m+1}}{(1+m+m\beta)^L}$$
$$\cdot \exp\left\{ \frac{-m\rho_l}{1+m+m\beta} \right\} \sum_{r=0}^{mL-m} C_r(m,L) \left[\frac{1+\beta}{1+m+m\beta} \right]^r \qquad (4.57)$$
$$\cdot \sum_{p=0}^{r} \frac{(\rho_l)^p}{p!(1+\beta)^p(1+m+m\beta)^p} \binom{p+L-1}{p-r}.$$

The noncentral parameter ρ_l for the rate = k/n coded waveform with l out of L channels jammed is

$$\rho_l = \frac{kK}{nL} \left[l \frac{E_b}{N_T} + (L-l) \frac{E_b}{N_0} \right], \qquad (4.58)$$

where $N_T = N_0 + N_J/\eta$ as before.

1. Convolutional codes

The convolution codes considered here are binary codes with constraint length 7, and a rates of 1/2 and 1/3. The Viterbi decoding algorithm is assumed and the information bit error rate for the best rate, constraint length 7 code can be bounded by the Chernoff bound. A best rate convolutional code is one that gives the best performance from a Viterbi decoder. [Ref. 15] For best rate 1/2 codes, the bound is

$$P_b \leq \frac{1}{2}(36D^{10} + 211D^{12} + 1404D^{14} + 11633D^{16} + \cdots), \qquad (4.59)$$

and for rate 1/3

$$P_b \leq \frac{1}{2}(7D^{15} + 8D^{16} + 22D^{17} + 44D^{18} + \cdots), \qquad (4.60)$$

where

$$D = 2\sqrt{P_c(1 - P_c)}\,. \tag{4.61}$$

In (4.61) P_c is the forward transition error of a binary symmetric channel, which for a binary code and a M-ary-to-Binary decoding is

$$P_c = \frac{M/2}{M - 1} P_s, \tag{4.62}$$

where P_s is given by (4.57). The higher order terms for D in (4.59) and (4.60) are neglected due to the usually small size of P_c

2. Reed-Solomon codes

Reed-Solomon codes were found to be particarly well suited for usage on fading channels, more so than convolutional codes because Viterbi decoders are not well-suited to the bursty errors associated with fading [Ref. 16]. The Reed-Solomon codes are non-binary linear block codes in which the elements of the code word are selected from Q symbols. Usually $Q = 2^q$ so that k information bits are mapped into one Q symbol. For $q > K$, where $K = \log_2 M$, q/K M-ary words are mapped to the Q-ary symbols and the symbol error at the output of the decoder is

$$P_c = 1 - (1 - p_s)^{q/K}. \tag{4.63}$$

In practice, q/K is usually an integer.

For an (k,n) block code, the decoder accepts an n-tuple of Q-ary coded symbols and outputs a k-tuple of decoded information symbols which are further broken down into information bits by the Q-ary-to-binary decoder. At the decoder output the probability of error for the Q-ary symbols is

$$P_q \cong \frac{d}{n} \sum_{i=t+1}^{d} \binom{n}{i} P_c^i (1 - P_c)^{n-i} + \frac{1}{n} \sum_{i=d+1}^{n} i \binom{n}{i} P_c^i (1 - P_c)^{n-i}, \tag{4.64}$$

where d is the minimum distance between code words, which for Reed-Solomon codes is $d = n - k + 1$, and

$$t = \left[\frac{d-1}{2} \right] \tag{4.65}$$

is the maximum number of correctable symbol errors in a code word. [Ref. 10] The notation $[x]$ denotes the integer less than or equal to x. The probablity of bit error is then given by

$$P_b = \frac{Q/2}{Q-1} P_q. \tag{4.66}$$

C. NUMERICAL RESULTS

In both the coded and uncoded cases, the generation of the probability of bit error involved a computer simulation of equation (4.53). In applying optimum partial band jamming, the jamming fraction η which maximized the probability of bit error had to be found. This was accomplished by performing a numerical search for η at each value of jamming power to noise power density ratio E_b/N_J for every value of m, L, E_b/N_0, and $\bar{\gamma}^2$.

1. Uncoded performance

Uncoded performance for various levels of fading are shown in Figures 11 to 14 for $E_b/N_0 = 10$ dB, and $M = 4$. Also plotted is the ideal performance for no fading or jamming with the abscissa as E_b/N_0 vice E_b/N_J. In comparing these curves for each value of η one can see the adverse effects fading has on the system performance. It can also be noted how diversity improves performance significantly for small value of $\bar{\gamma}^2$ (Rayliegh fading), but the diversity also hinders performance when there is a strong direct component in the received signal (high $\bar{\gamma}^2$). At $\bar{\gamma}^2 = 15$ the performance of all levels of diversity are about the same. For a signal-to-noise ratio of 15 dB, a similar result is seen in Figures 15 and 16. For the higher E_b/N_0, however, the adverse effects of diversity are not realized in that the higher E_b/N_0 offsets the recombining losses. Figures 17 and 18 show a comparison of performance for various values of M when $L = 2$ and $E_b/N_0 = 10$ dB,

for both the Rayleigh fading case and a Rician fading case respectively. From these curves it is apparent that an increased symbol size gives better performance. More improvement from diversity is seen in the Rician channel.

2. Coded performance

The first convolutional code considered was a best rate 1/2, constraint length-7 code with the probability of bit error bounded by (4.59). Plots of the error rates for this code are shown in Figures 19, 20, 21, and 22 for various levels of fading with $M = 4$ and $E_b/N_0 = 15$ dB in worst case partial band jamming. In the non-fading and Rician fading with a strong direct component cases ($\overline{\gamma}^2 = 15$) (see Figures 19 and 20), the optimum level of diversity is $L = 2$ hops per symbol. However, as the fading becomes stronger (see Figures 21 and 22), the performance increases when there are a greater number of hops per symbol. This is as expected, if these plots are compared with the results for the uncoded system in which the higher levels of diversity increased performance as fading increased. Furthermore, a comparision of Figures 20 and 22 with Figures 15 and 16 shows that coding does indeed decrease error rates as expected. For binary-FSK modulation ($M = 2$), the same general pattern is evident (see Figures 23 and 24) where diversity improves performance as fading increases. Also, a comparison of the BFSK results with the MFSK results indicate that better performance is gained with higher values of M.

The best rate 1/3 constraint length-7 code results are shown in Figures 25 and 26 for Rayleigh fading and Rician fading when $M = 2$ and $E_b/N_0 = 15$ dB. Again one can see that the greater number of hops per symbol provide increased performance in deep fading. With the rate 1/3 code, however, slow hopping ($L = 1$) provides consistently poor performance, even with no fading. A (15,8) Reed-Solomon code was used to generate the curves in Figures 27 and 28 for $M = 4$ and $E_b/N_0 = 15$ dB in Rician and Rayleigh fading channels respectively. The probability of bit error for this code is given by (4.63) through (4.66) with $d = 8$ and $t = 3$. Therefore, the (15,8) code has an error correction capability of 3 bits.

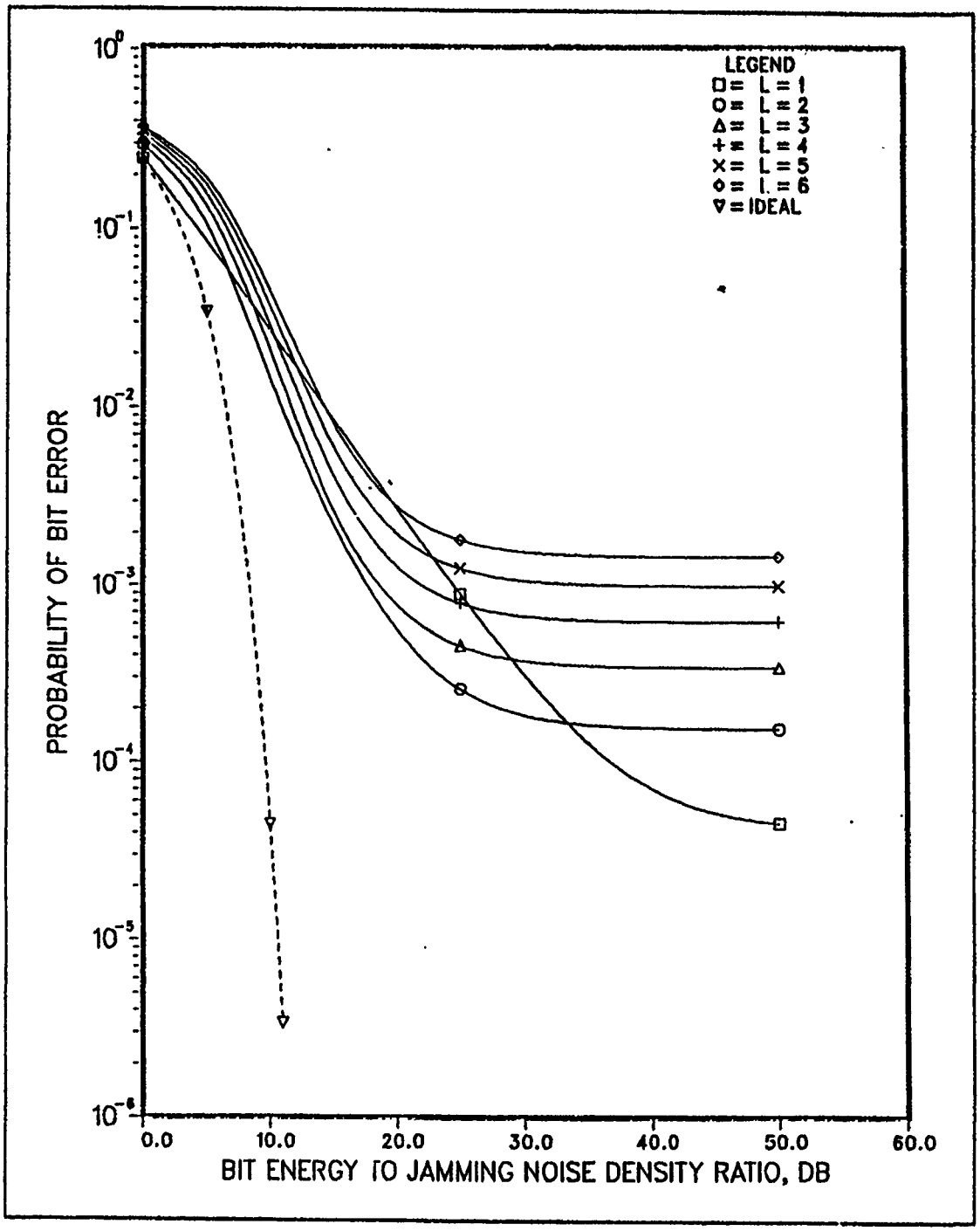

Figure 11. **Performance of receiver for no fading:** $\overline{\gamma^2} = \infty$ and $M = 4$ under optimum partial-band jamming conditions with number of hops-per- symbol (L) as a parameter when $E_b/N_0 = 10$ dB.

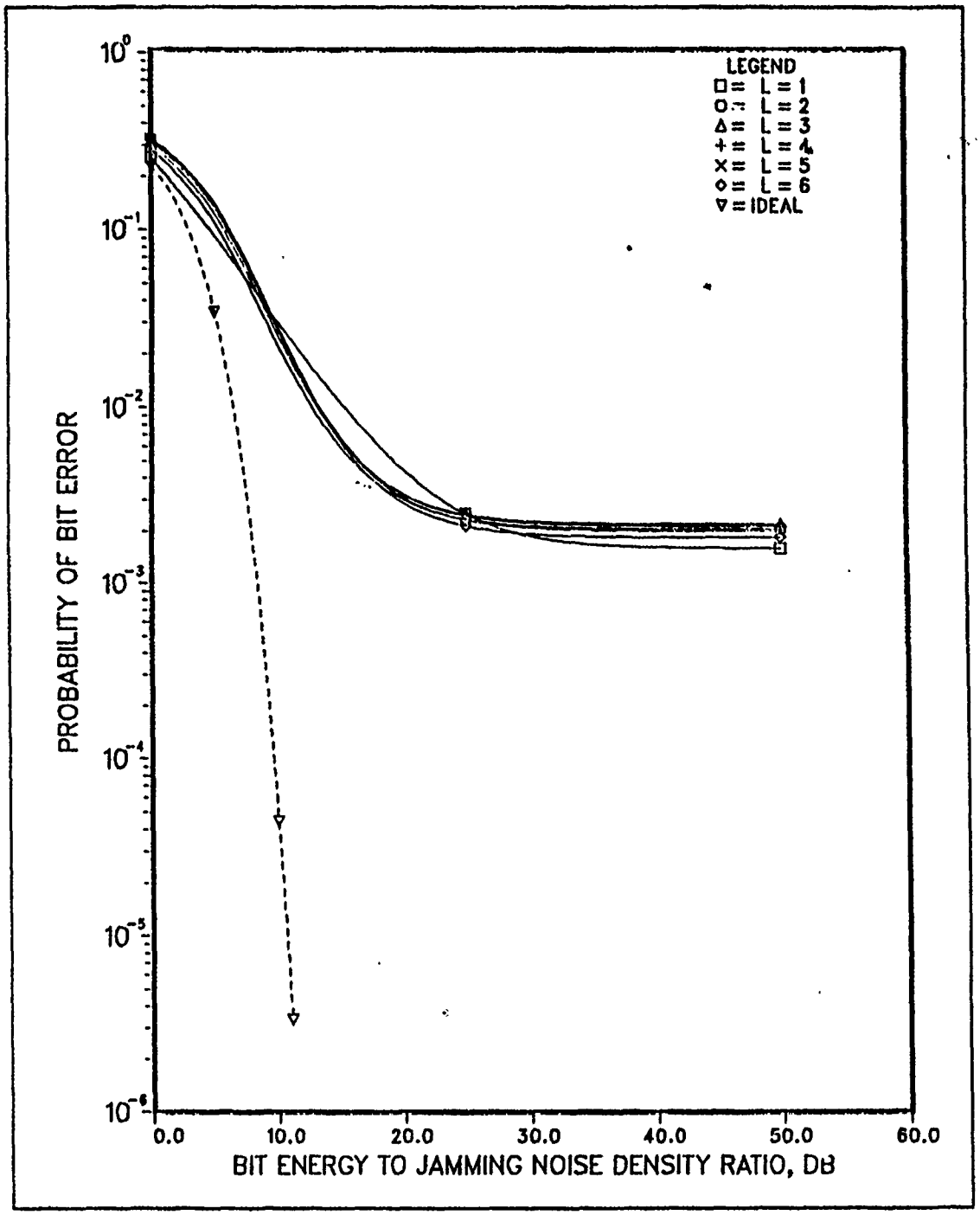

Figure 12. **Performance of receiver for Rician fading:** $\bar{\gamma}^2 = 15$ and $M = 4$ under optimum partial-band jamming conditions with number of hops-per-symbol (L) as a parameter when $E_b/N_0 = 10$ dB.

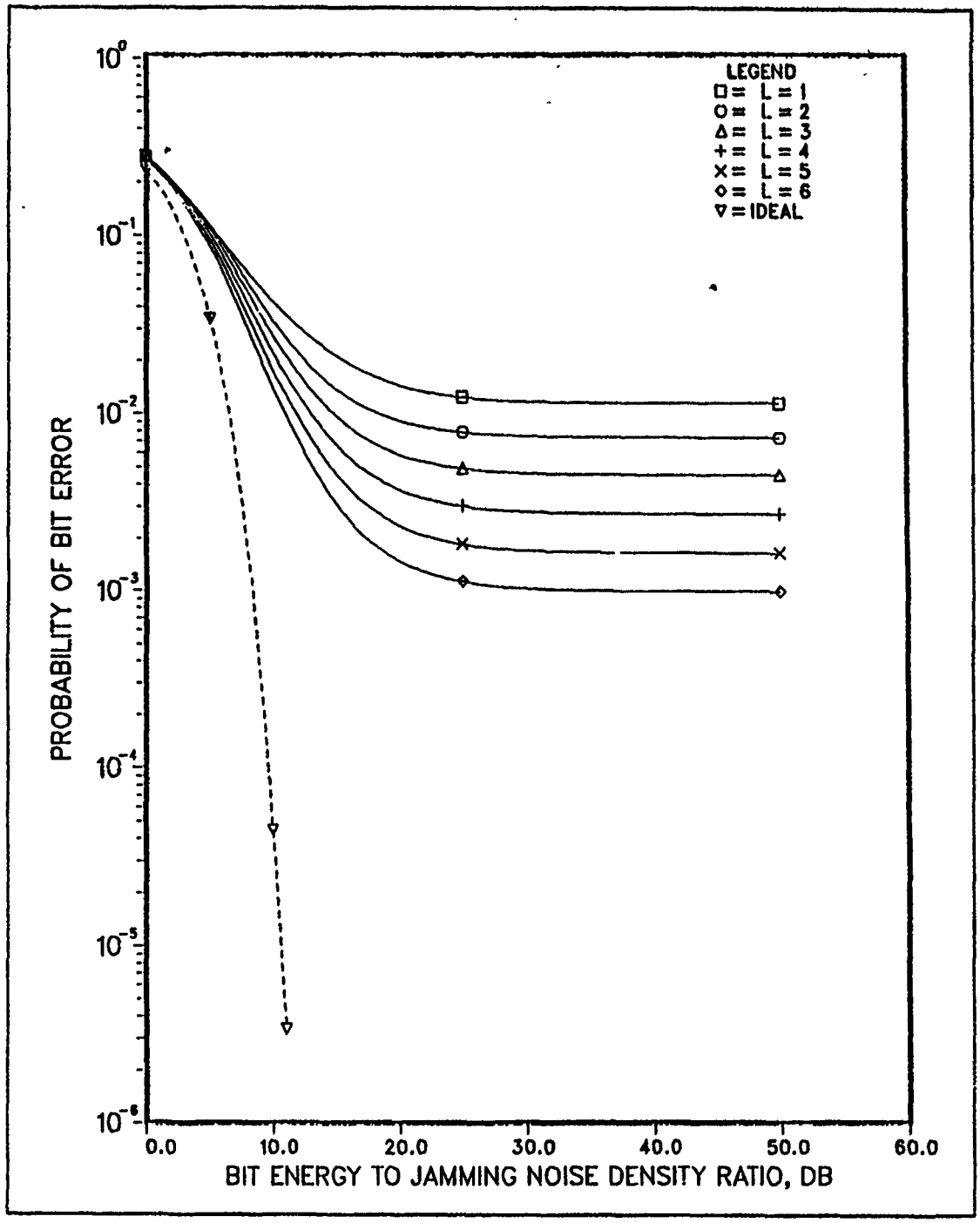

Figure 13. **Performance of receiver for Rician fading:** $\bar{\gamma}^2 = 5$ and $M = 4$ under optimum partial-band jamming conditions with number of hops-per-symbol (L) as a parameter when $E_b/N_0 = 10$ dB.

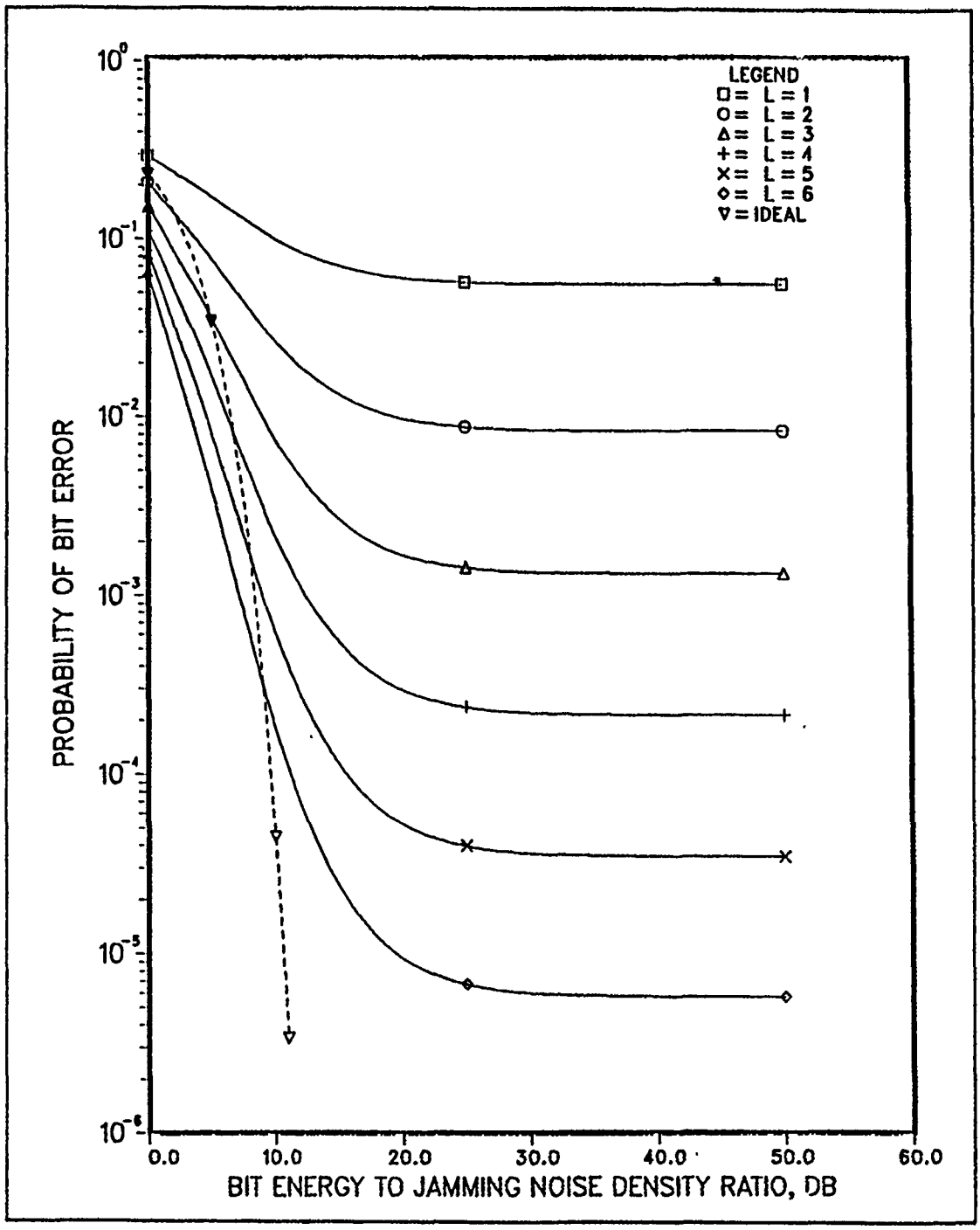

Figure 14. Performance of receiver for Rayleigh fading: $\bar{\gamma}^2 = 0$ and $M = 4$ under optimum partial-band jamming conditions with number of hops-per-symbol (L) as a parameter when $E_b/N_0 = 10$ dB.

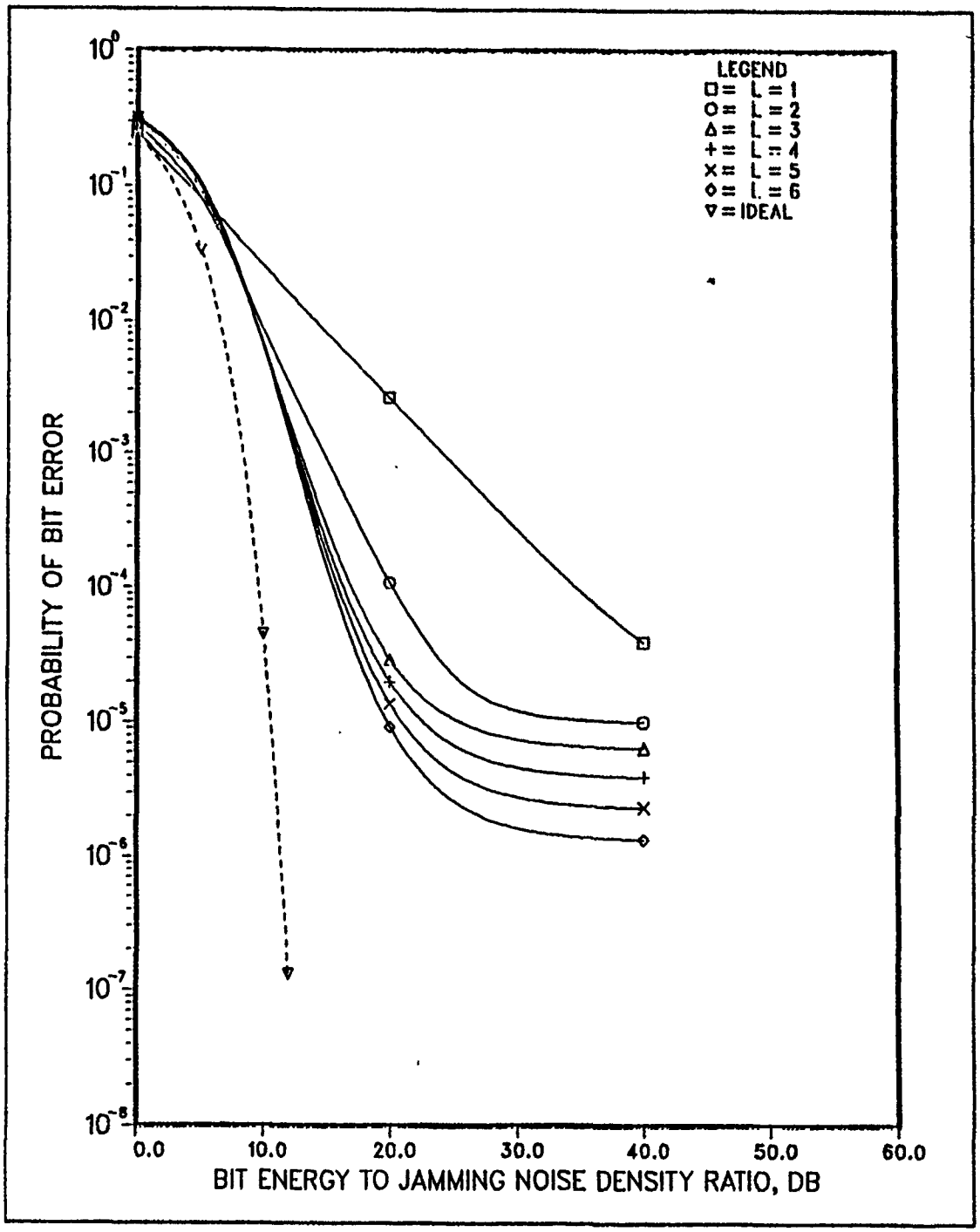

Figure 15. **Performance of receiver for Rician fading:** $\bar{\gamma}^2 = 15$ and $M = 4$ under optimum partial-band jamming conditions with number of hops-per-symbol (L) as a parameter when $E_b/N_0 = 15$ dB.

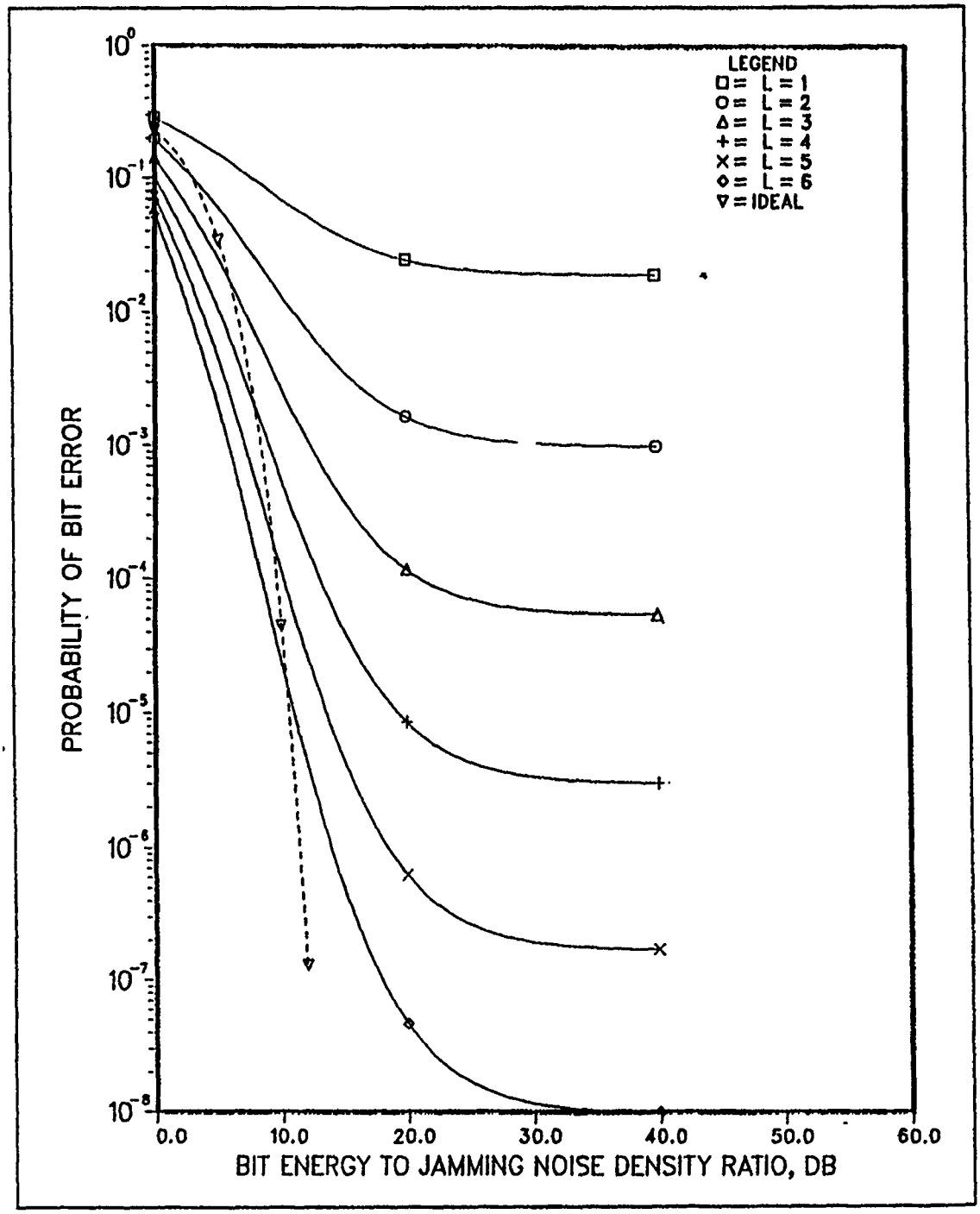

Figure 16. Performance of receiver for Rayleigh fading: $\bar{\gamma}^2 = 0$ and $M = 4$ under optimum partial-band jamming conditions with number of hops-per-symbol (L) as a parameter when $E_b/N_0 = 15$ dB.

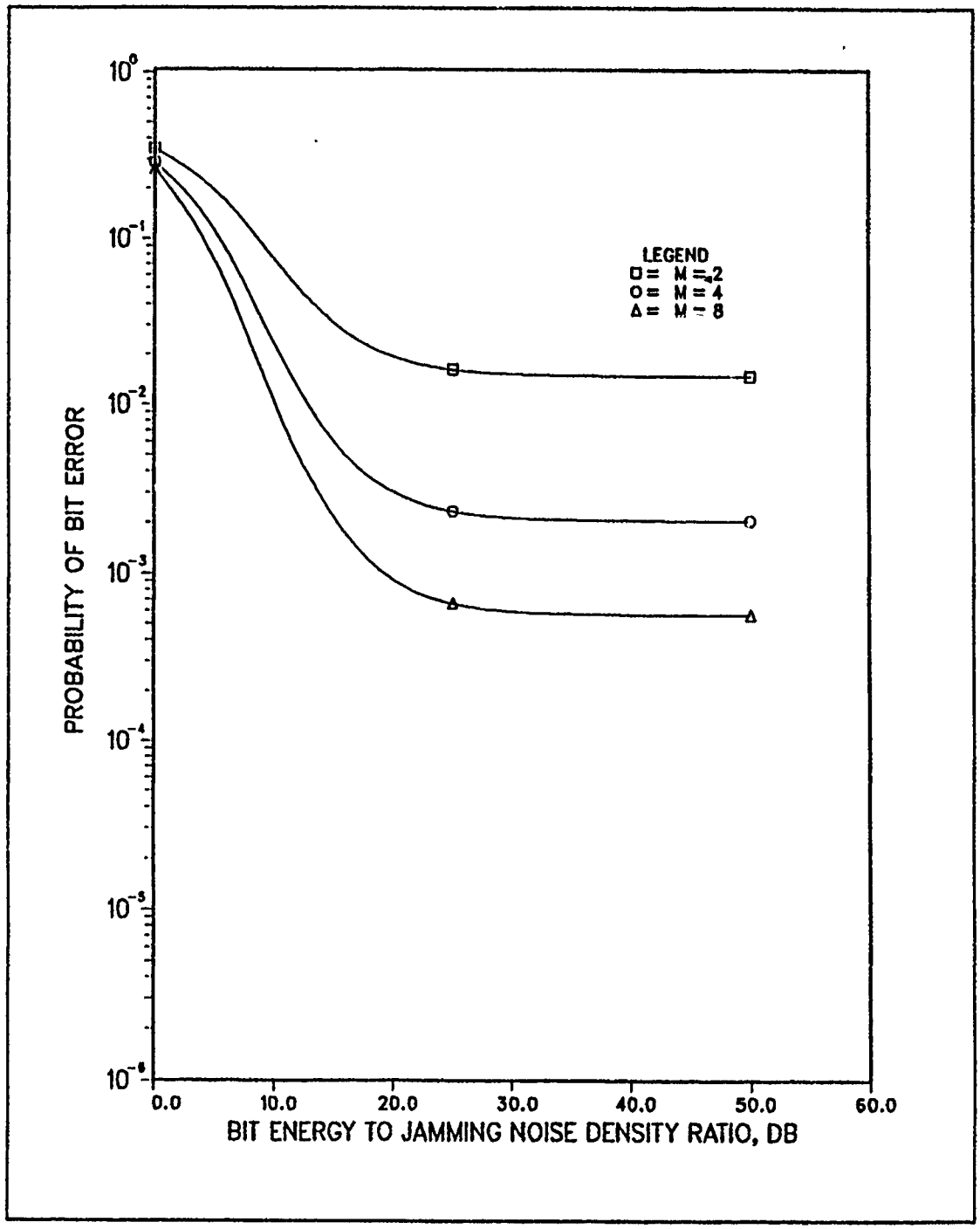

Figure 17. **Performance of receiver for Rician fading:** $\bar{\gamma}^2 = 15$ and $L = 2$ under optimum partial-band jamming conditions with number of hops-per-symbol (M) as a parameter when $E_b/N_0 = 10$ dB.

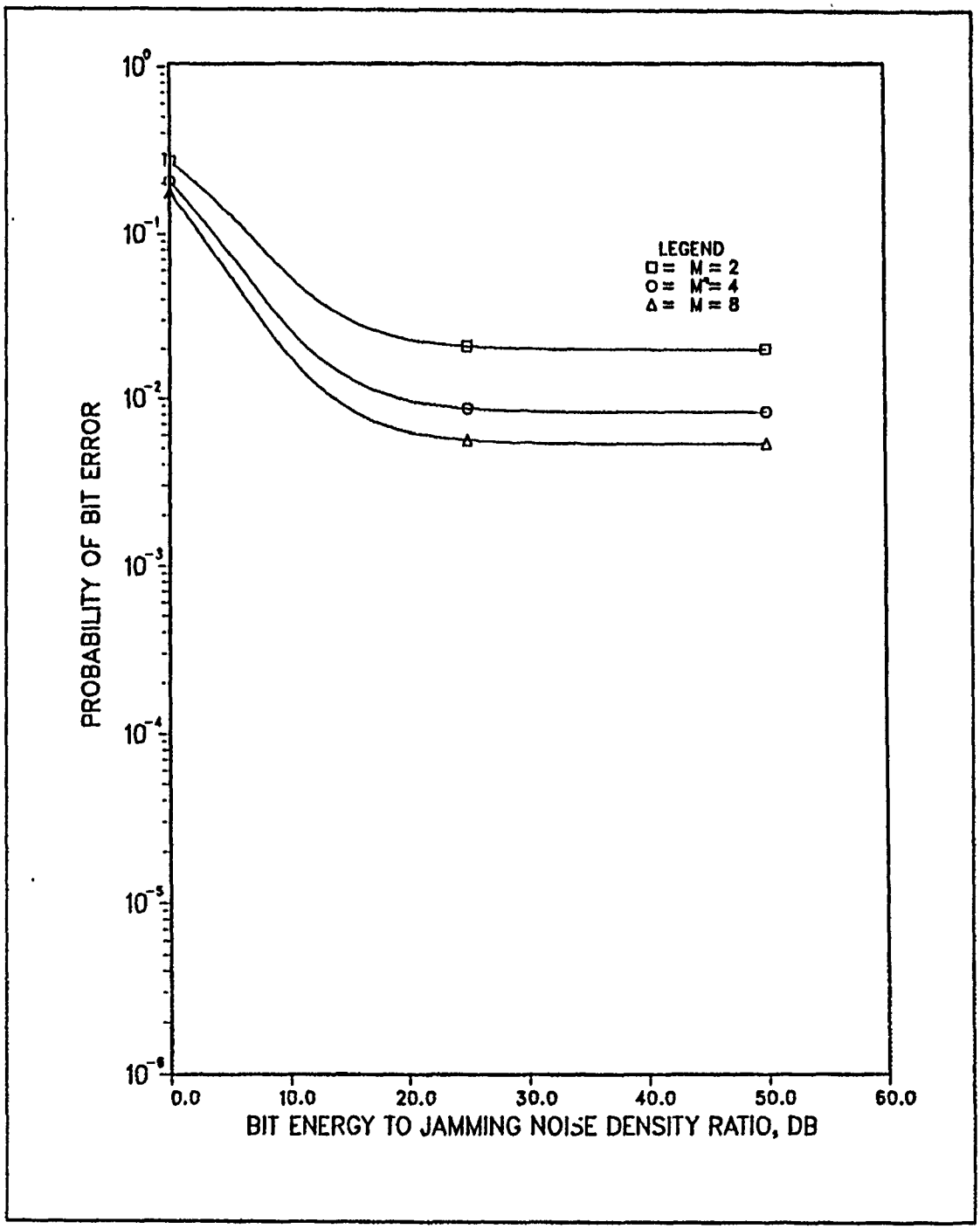

Figure 18. Performance of receiver for Rayleigh fading: $\bar{\gamma}^2 = 0$ and $L = 2$ under optimum partial-band jamming conditions with number of hops-per-symbol (M) as a parameter when $E_b/N_0 = 10$ dB.

All three codes discussed are plotted together in Figures 29 to 32 for two levels of diversity, $L = 2$ (solid line), and $L = 3$ (dashed line), when $M = 4$ and $E_b/N_0 = 15$ dB. From the curves one can see that the best rate 1/2 convolutional code consistently provides better detection capabilities than the other two. In addition, the rate 1/3 convolutional code is slightly better than the Reed-Solomon (15,8) code for signals with strong direct components, and much better for signals in deeper fading. Here again, the benifits of diversity can be seen as the amount of fading increases.

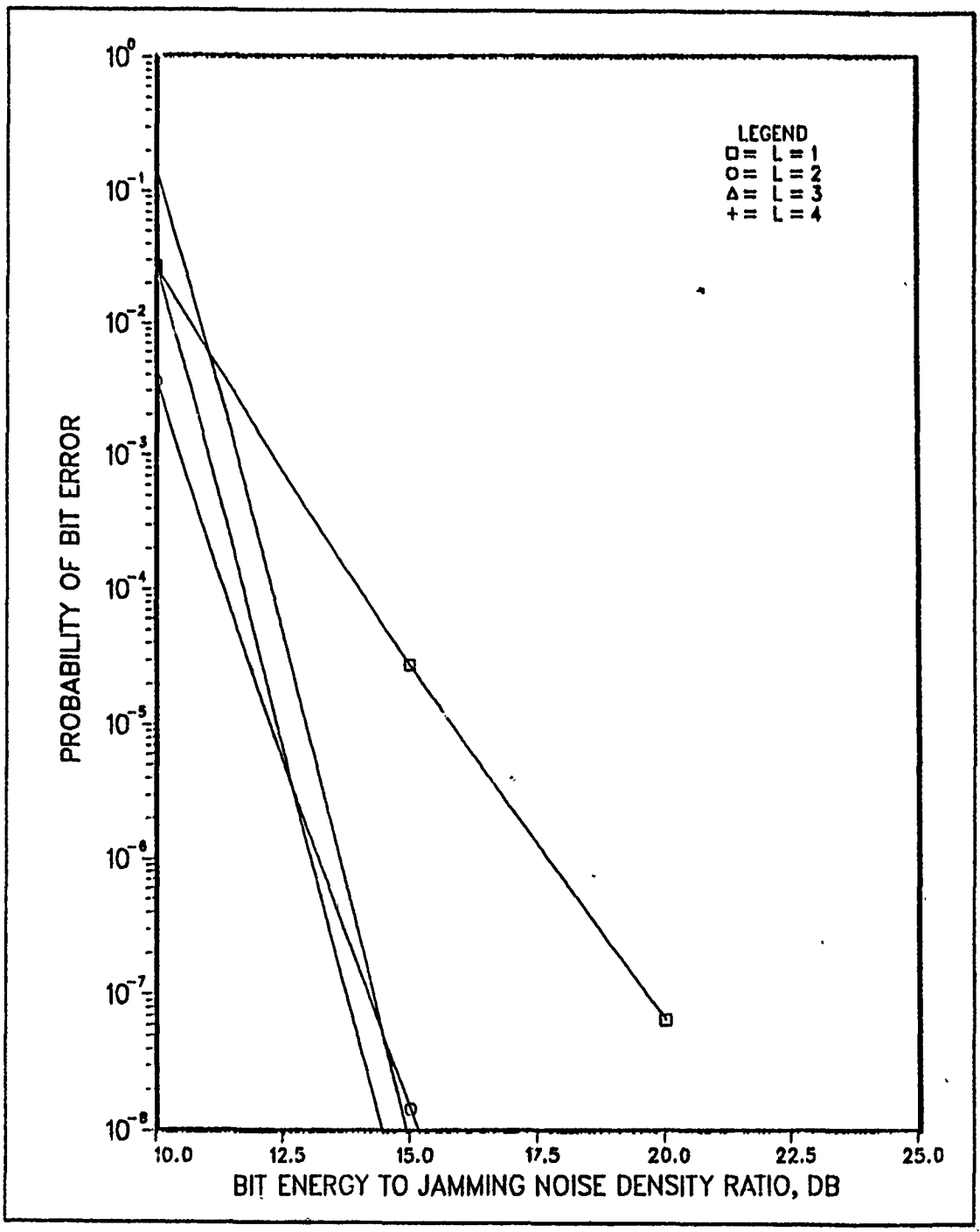

Figure 19. **Performance of rate 1/2 convolutional code with no fading:** $\overline{\nu^2} = \infty$ and $M = 4$ under optimum partial-band jamming conditions with number of hops-per- symbol (L) as a parameter when $E_b/N_0 = 15$ dB.

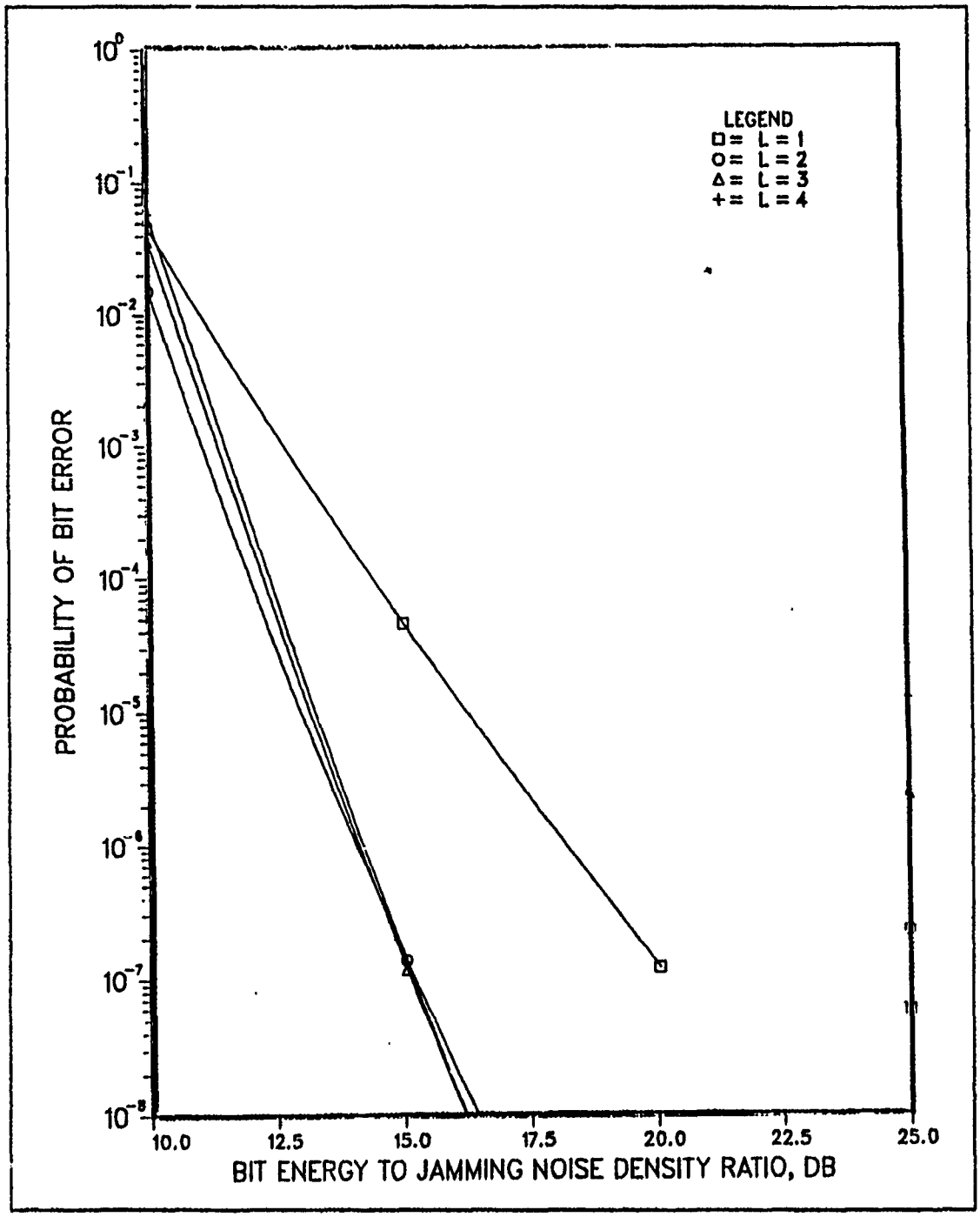

Figure 20. **Performance of rate 1/2 convolutional code in Rician fading:** $\overline{\gamma}^2 = 15$ and $M = 4$ under optimum partial-band jamming conditions with number of hops-per- symbol (L) as a parameter when $E_b/N_0 = 15$ dB.

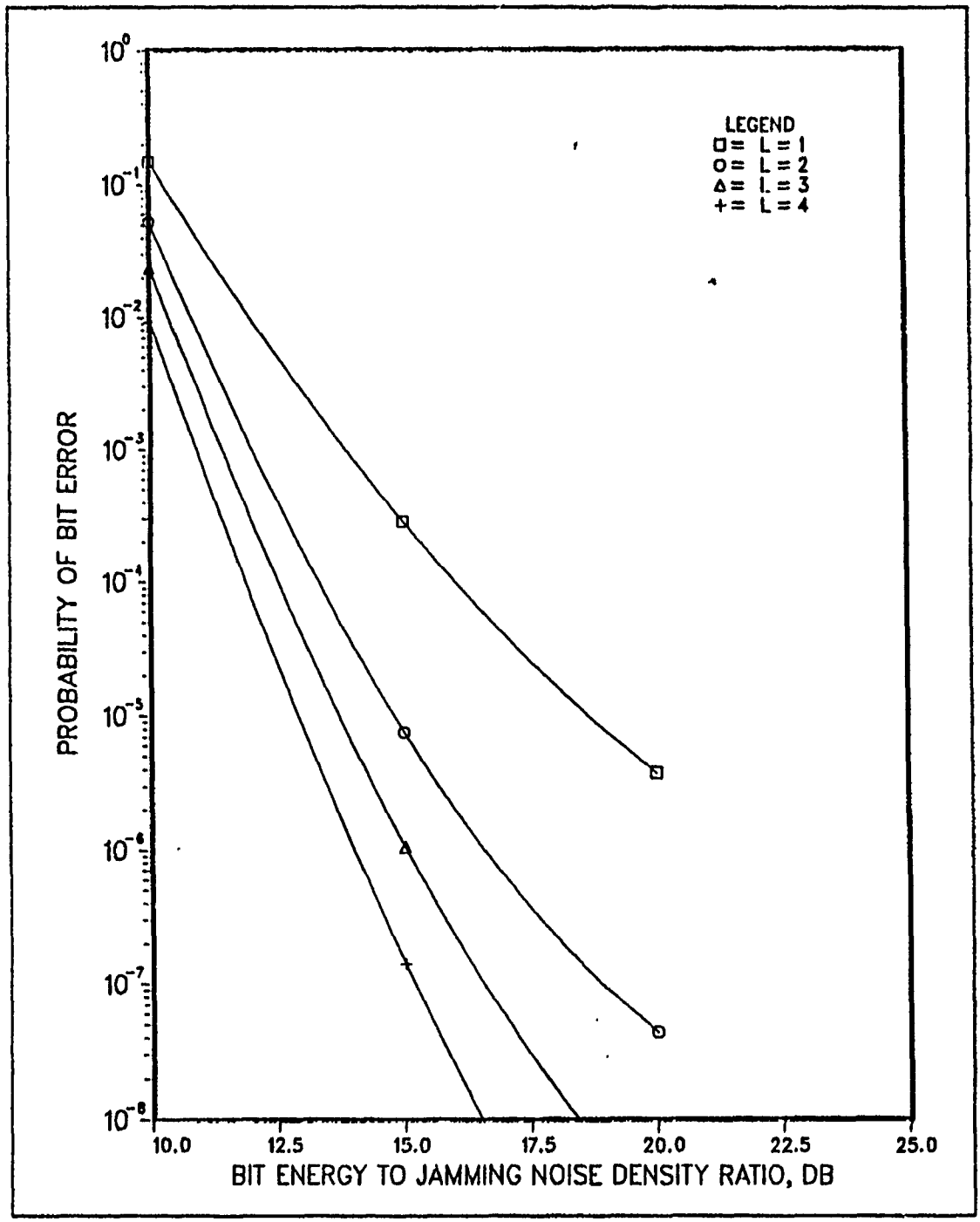

Figure 21. **Performance of rate 1/2 convolutional code in Rician fading:** $\overline{\gamma}^2 = 5$ and $M = 4$ under optimum partial-band jamming conditions with number of hops-per- symbol (L) as a parameter when $E_b/N_0 = 15$ dB.

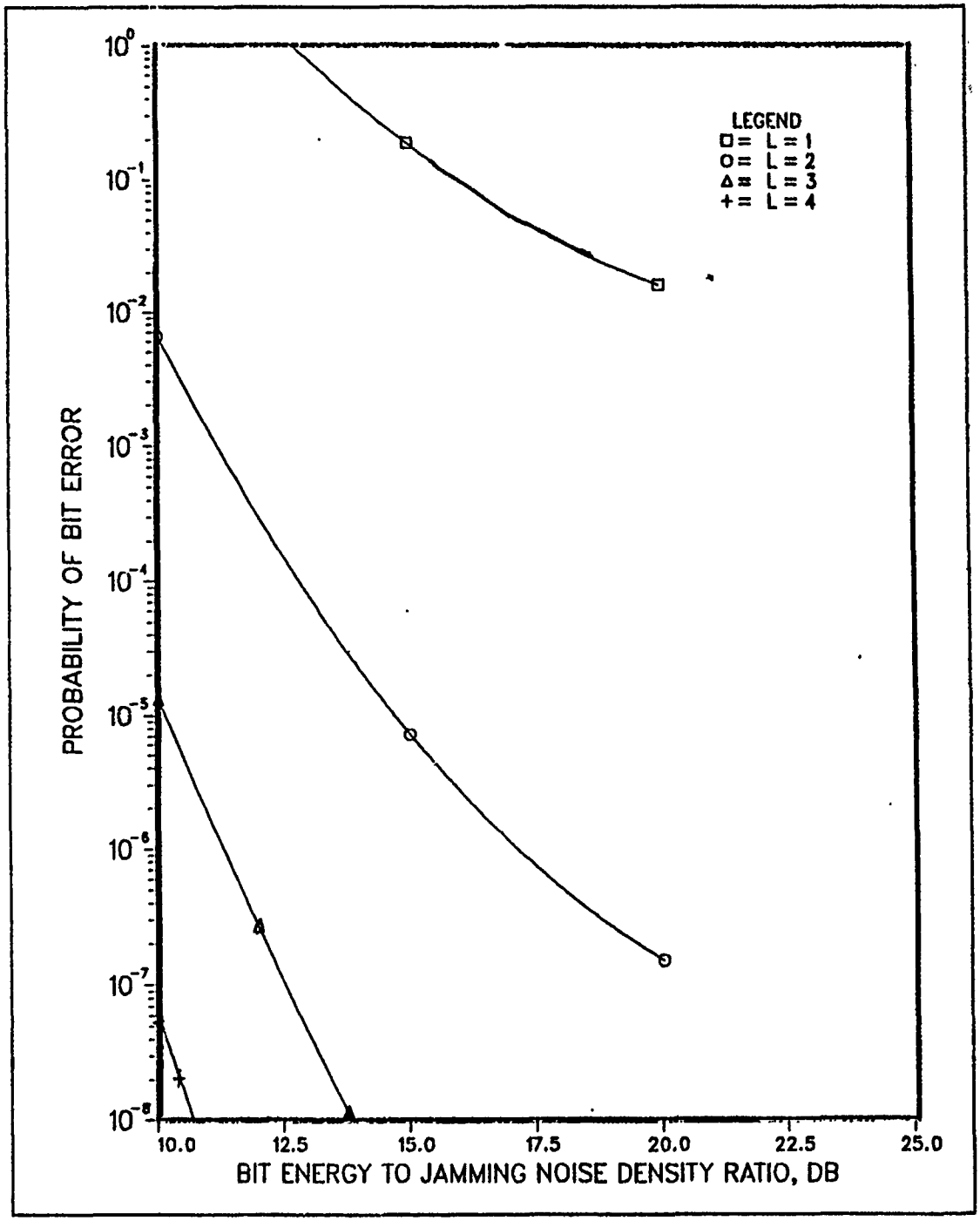

Figure 22. **Performance of rate 1/2 convolutional code in Rayleigh fading:** $\bar{\gamma}^2 = 0$ and $M = 4$ under optimum partial-band jamming conditions with number of hops-per-symool (L) as a parameter when $E_b/N_0 = 15$ dB.

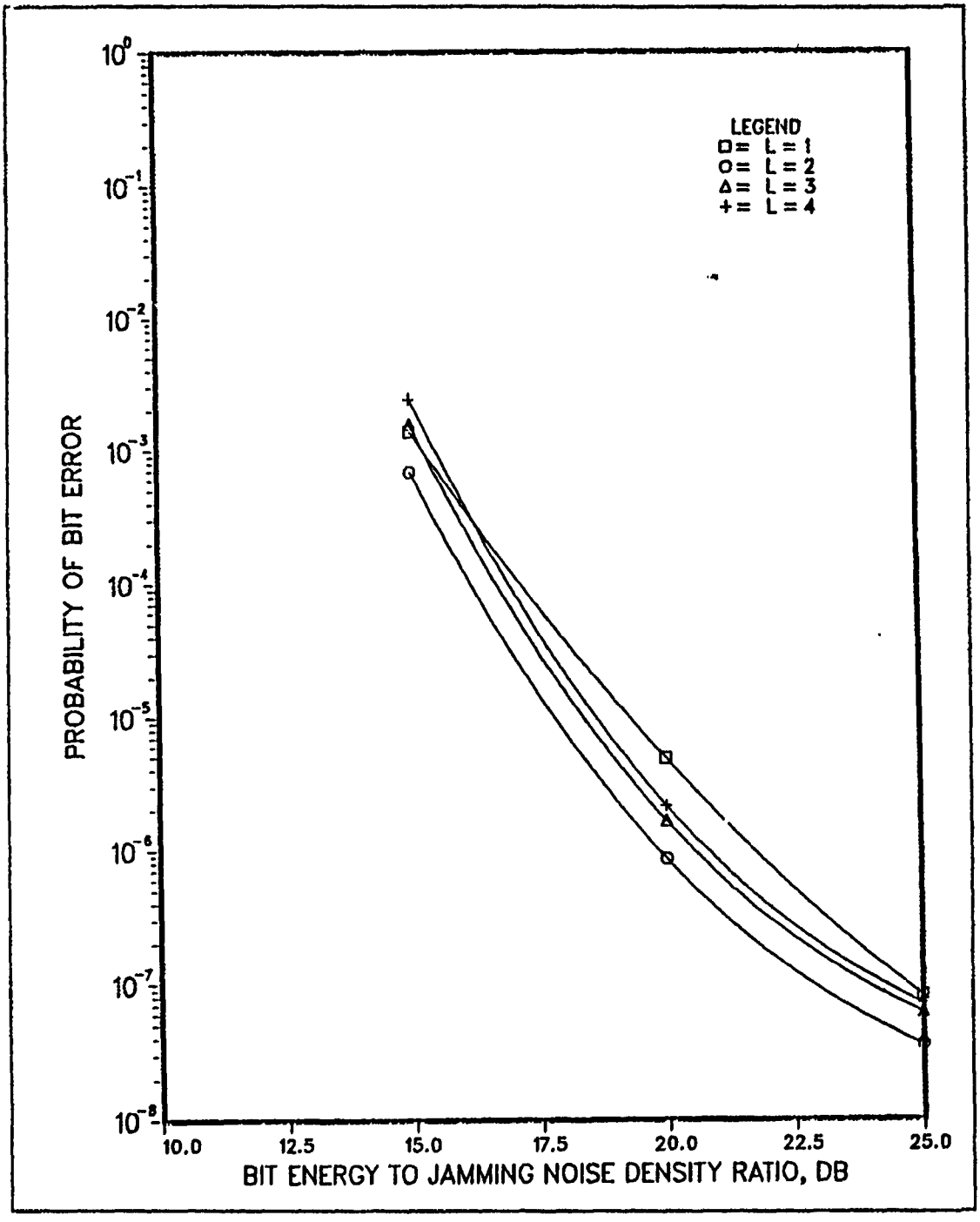

Figure 23. **Performance of rate 1/2 convolutional code in Rician fading:** $\bar{\gamma}^2 = 15$ and $M = 2$ under optimum partial-band jamming conditions with number of hops-per- symbol (L) as a parameter when $E_b/N_0 = 15$ dB.

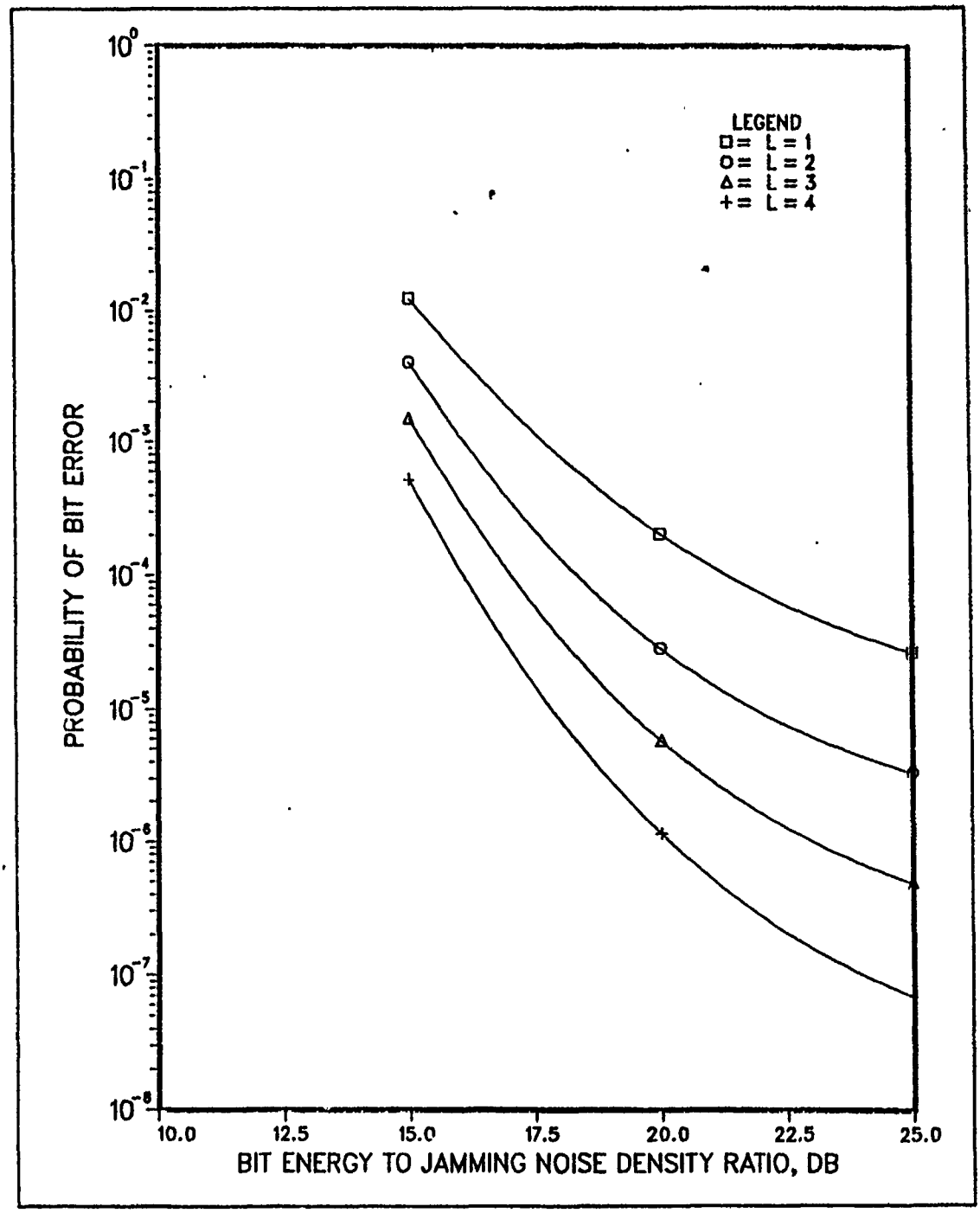

Figure 24. Performance of rate 1/2 convolutional code in Rician fading: $\bar{\gamma}^2 = 5$ and $M = 2$ under optimum partial-band jamming conditions with number of hops-per-symbol (L) as a parameter when $E_b/N_0 = 15$ dB.

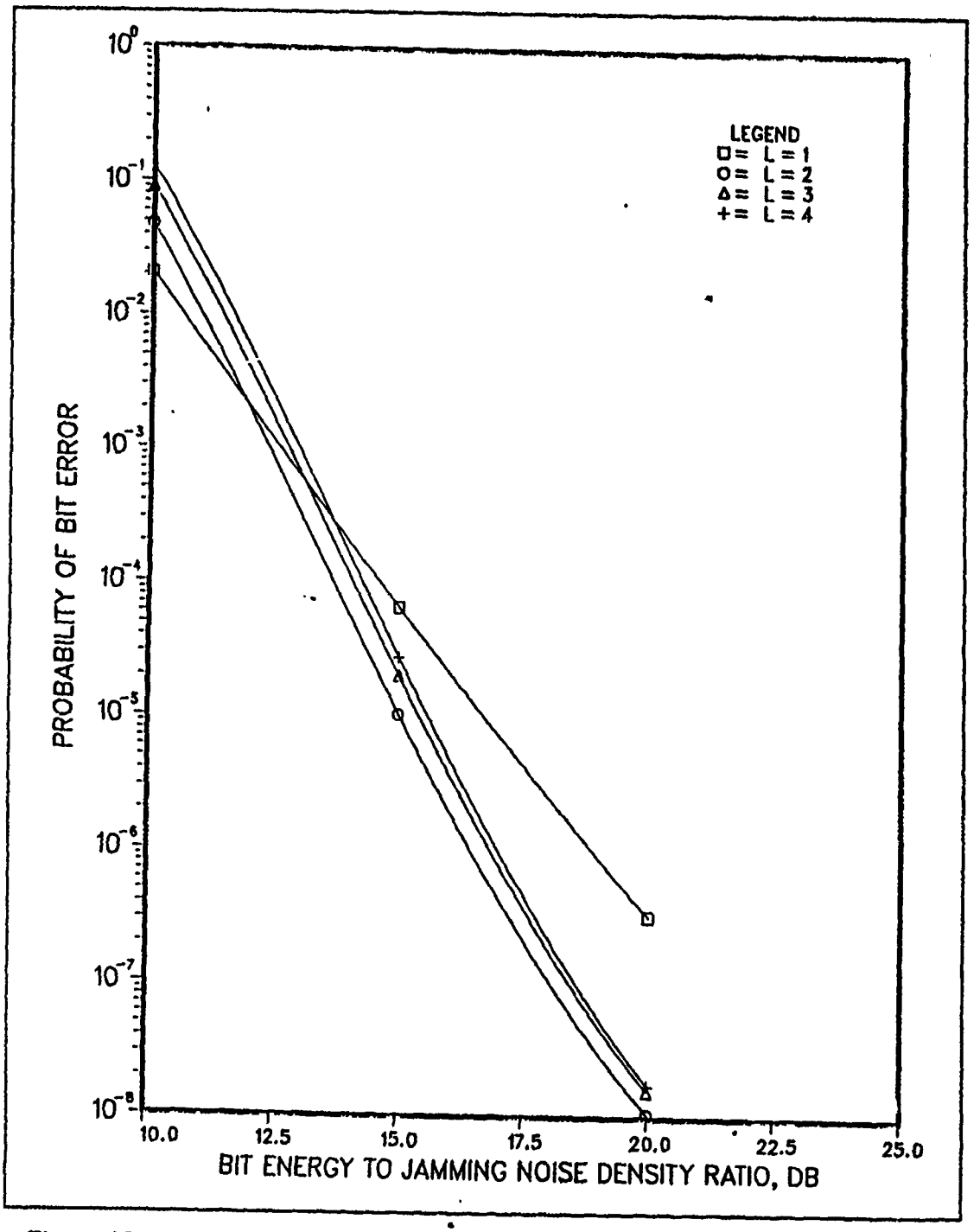

Figure 25. **Performance of rate 1/3 convolutional code in Rician fading:** $\overline{\gamma}^2 = 15$ and $M = 4$ under optimum partial-band jamming conditions with number of hops-per- symbol (L) as a parameter when $E_b/N_0 = 15$ dB.

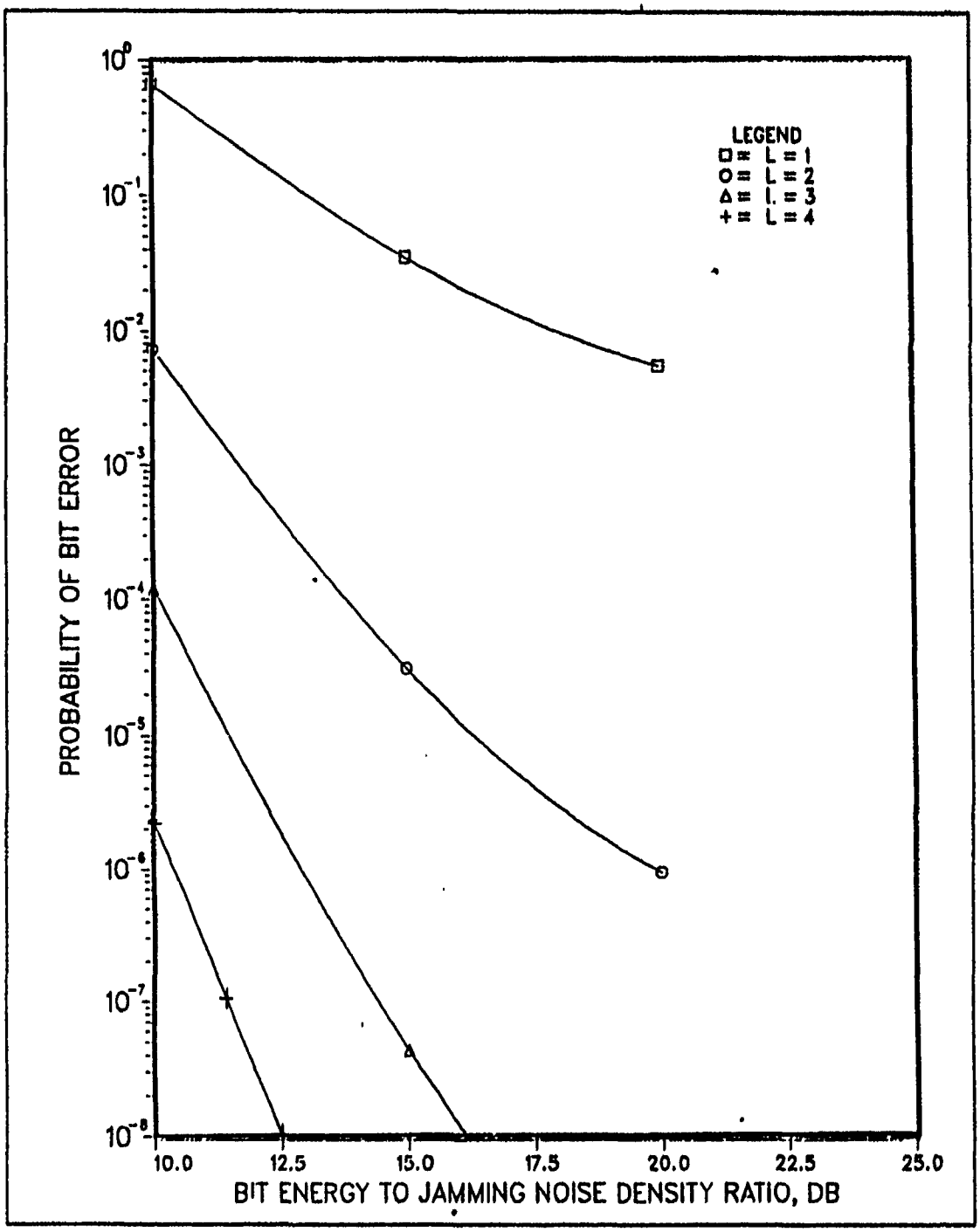

Figure 26. **Performance of rate 1/3 convolutional code in Rayleigh fading:** $\bar{\gamma}^2 = 0$ and $M = 4$ under optimum partial-band jamming conditions with number of hops-per- symbol (L) as a parameter when $E_b/N_0 = 15$ dB.

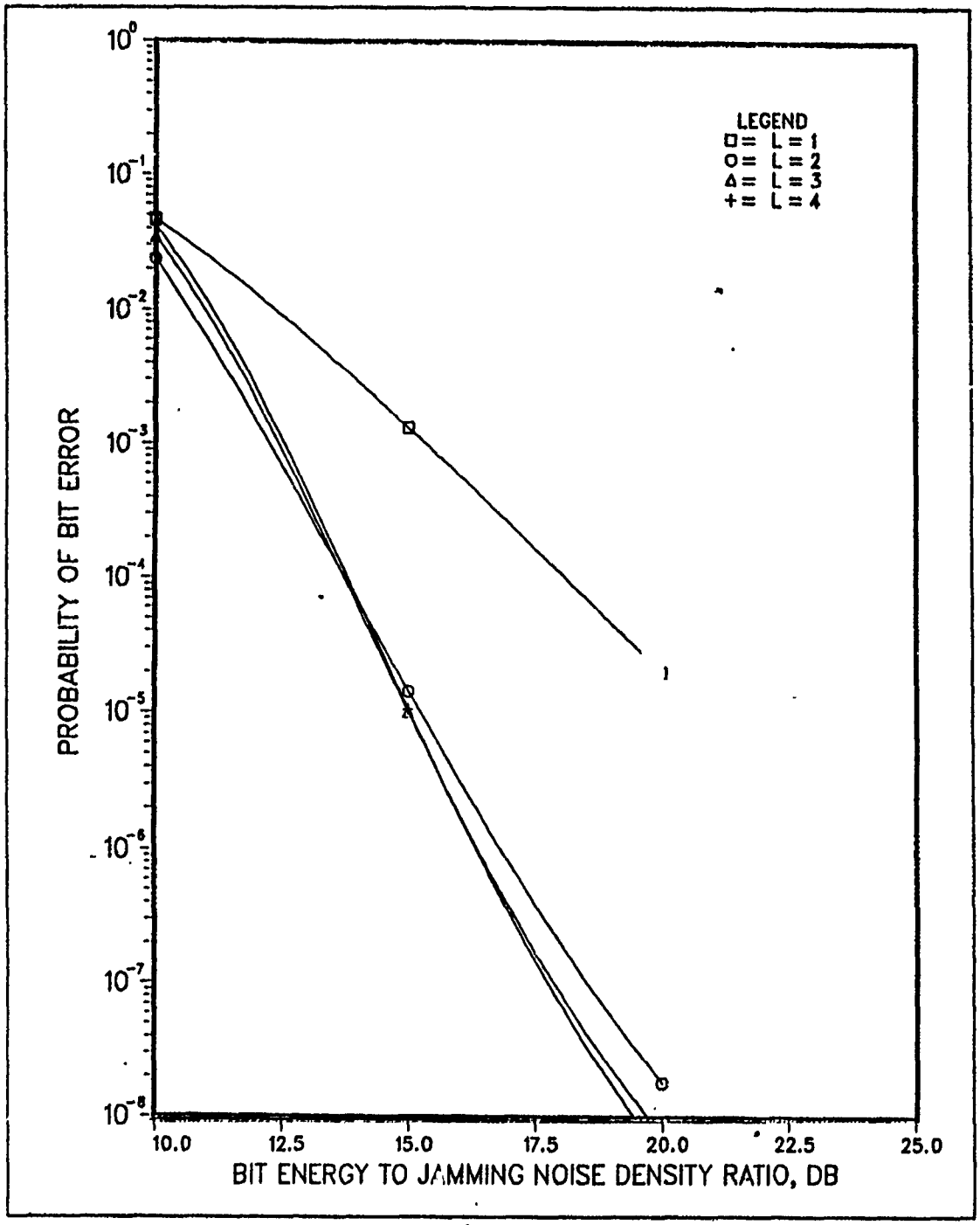

Figure 27. **Performance of Reed-Solomon (15,8) code in Rician fading:** $\bar{\gamma}^2 = 15$ and $M = 4$ under optimum partial-band jamming conditions with number of hops-per- symbol (L) as a parameter when $E_b/N_0 = 15$ dB.

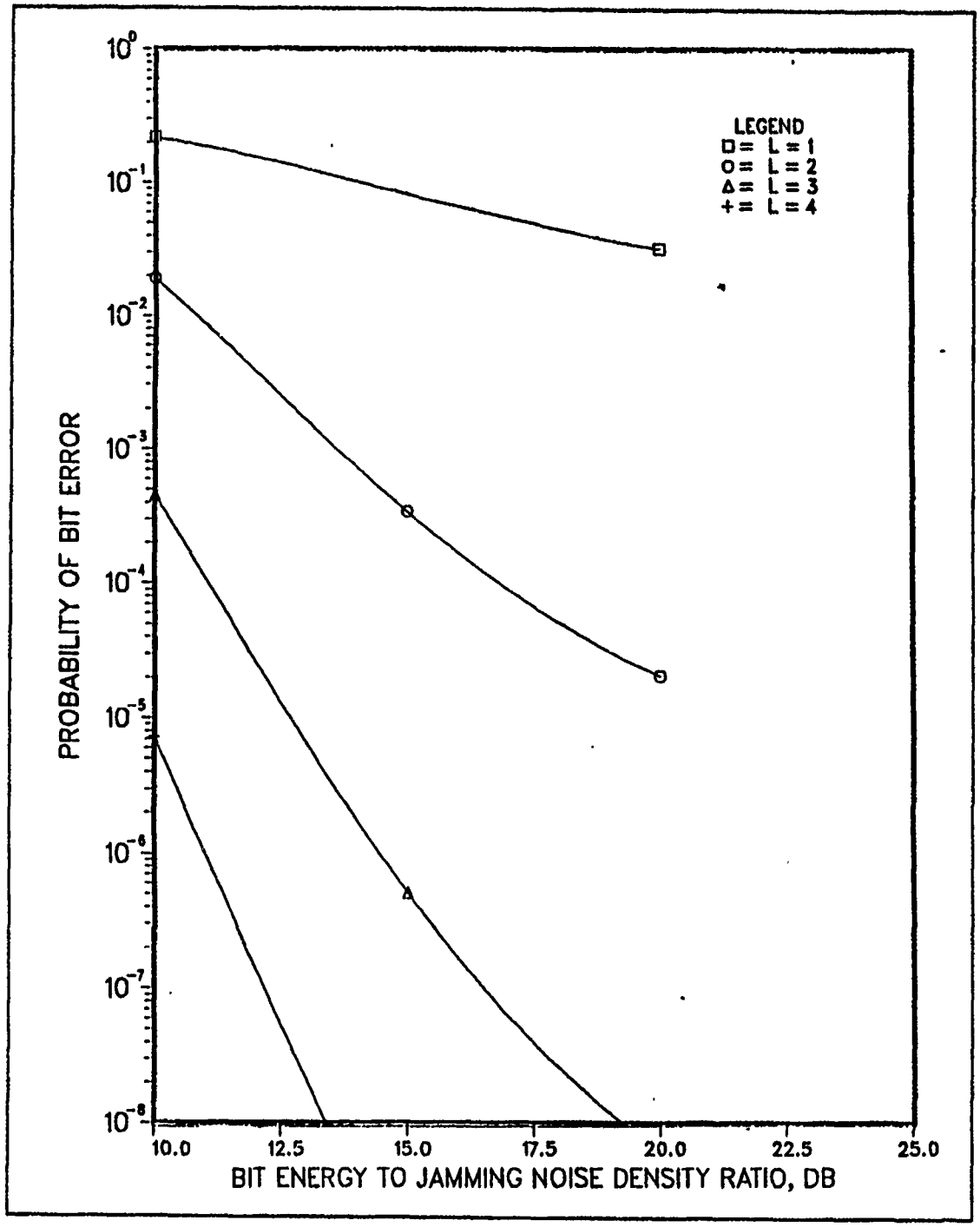

Figure 28. **Performance of Reed-Solomon (15,8) code in Rayleigh fading:** $\bar{\gamma}^2 = 0$ and $M = 4$ under optimum partial-band jamming conditions with number of hops-per- symbol (L) as a parameter when $E_b/N_0 = 15$ dB.

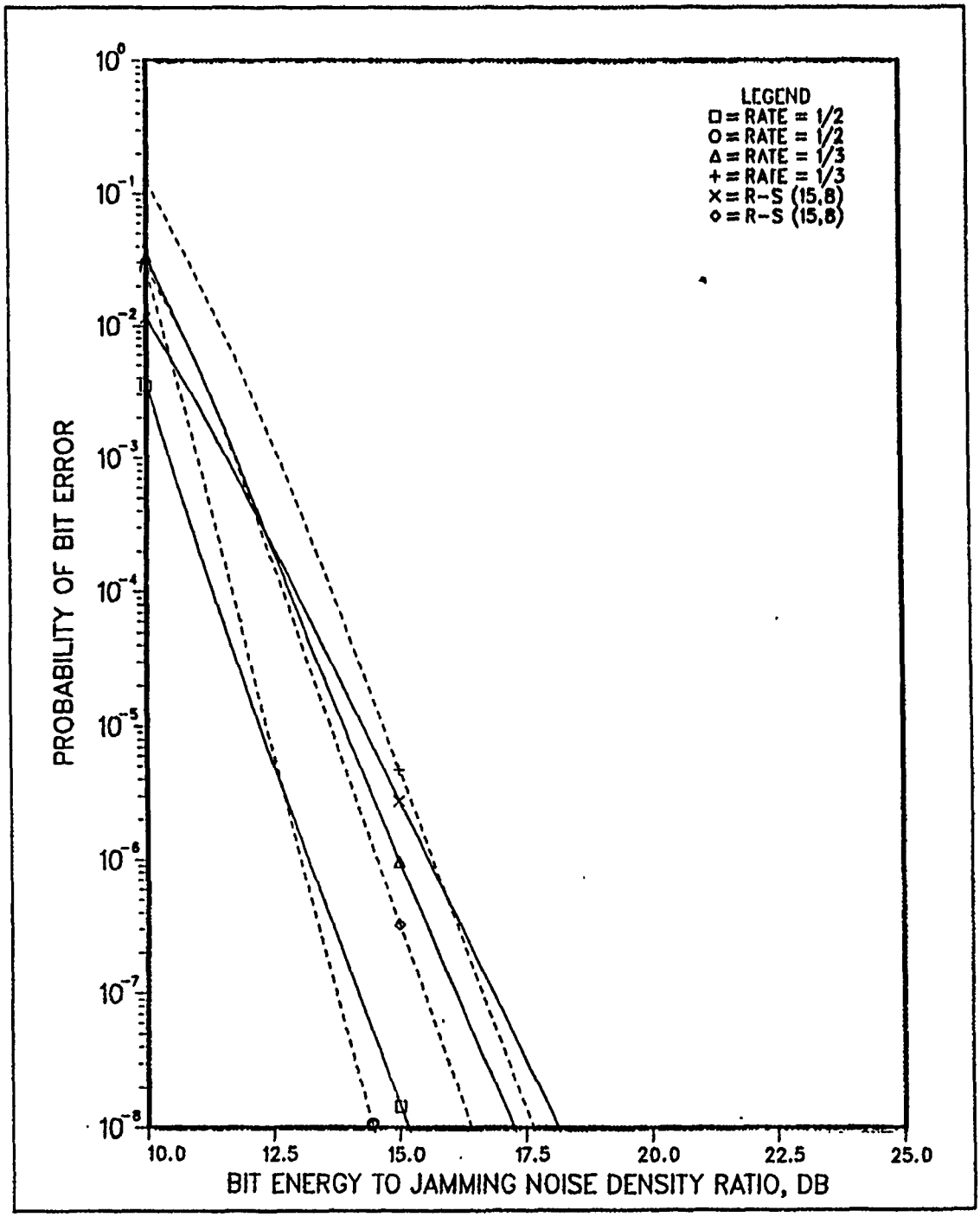

Figure 29. **Performance comparision of codes with no fading:** $\overline{\gamma}^2 = \infty$ and $M = 4$ under optimum partial-band jamming conditions with $L = 2$ (solid line) and $L = 3$ (dashed line) when $E_b/N_0 = 15$ dB.

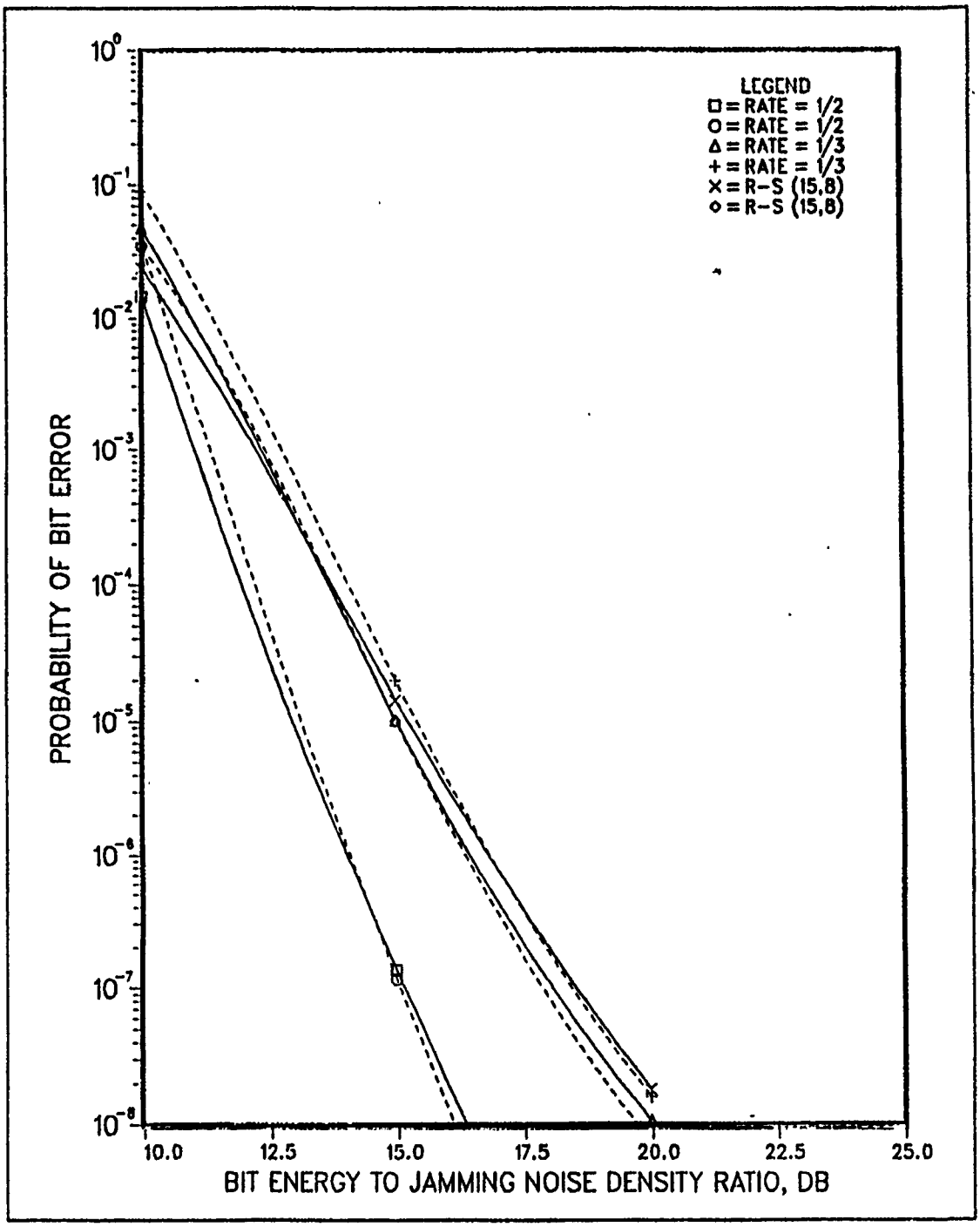

Figure 30. Performance comparision of codes in Rician fading: $\bar{\gamma}^2 = 15$ and $M = 4$ under optimum partial-band jamming conditions with $L = 2$ (solid line) and $L = 3$ (dashed line) when $E_b/N_0 = 15$ dB.

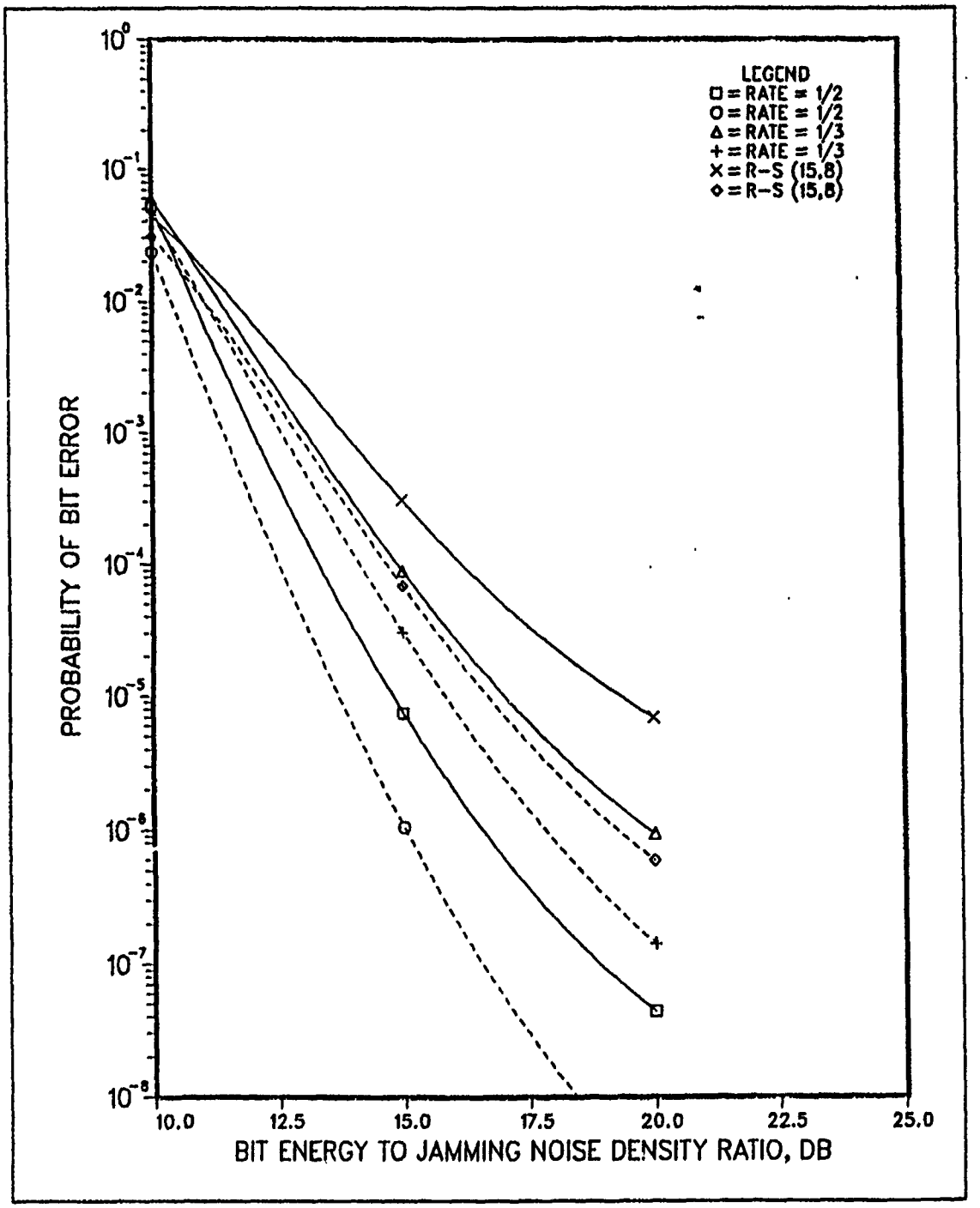

Figure 31. Performance comparision of codes in Rician fading: $\overline{\gamma}^2 = 5$ and $M = 4$ under optimum partial-band jamming conditions with $L = 2$ (solid line) and $L = 3$ (dashed line) when $E_b/N_0 = 15$ dB.

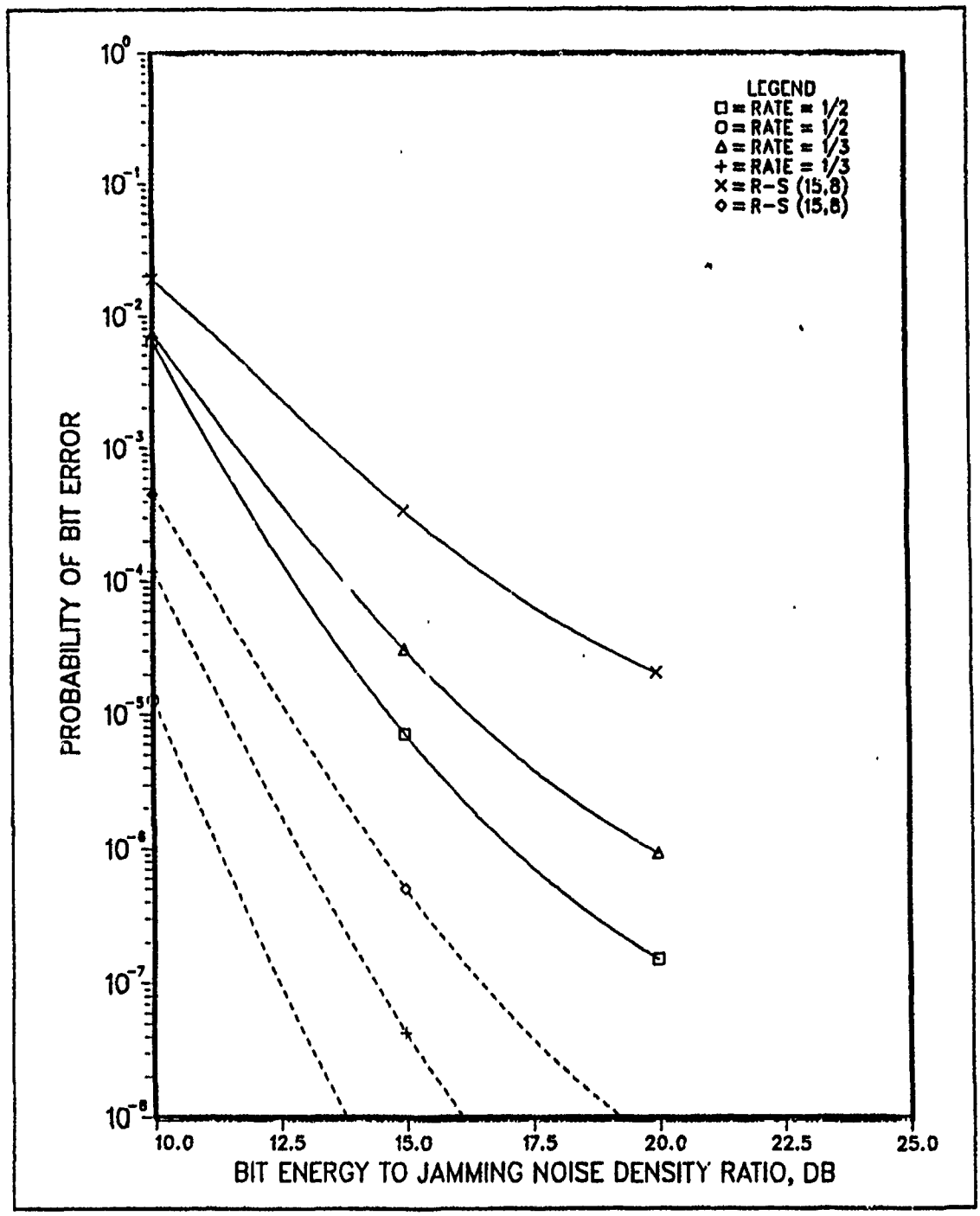

Figure 32. **Performance comparision of codes in Rayleigh fading:** $\overline{\gamma^2} = 0$ and $M = 4$ under optimum partial-band jamming conditions with $L = 2$ (solid line) and $L = 3$ (dashed line) when $E_b/N_0 = 15$ dB.

V CONCLUSIONS AND RECOMMENDATIONS

A. CONCLUSIONS

The theoretical study and numerical simulation of randomly spaced satellites indicate that there will usually be many satellites within communication range of a ground terminal with relatively few periods where coverage is not available. The large numbers of satellites could lead to high levels of interference and many multipath channels if no processing of signals or directional transmission of signals is performed. Furthermore, as the range between ground terminals desiring to communicate increases, the number of satellites available to communicate through decreases exponentially. This could lead to longer periods of no communication ability when the satellites are not equipped with a cross-link capability. For a 250 satellite array, from five to 20 satellites can be expected within range about 95% of the time.

The theory needed to analyze the performance of a fast-frequency-hopped MFSK system with side information in a fading channel and optimum partial band jamming has been developed. In the configurations considered, diversity and coding both provide improvement in system performance. The system is expected to operate in a fading channel and will thus require diversity and coding for improved performance. The optimum level of diversity for most combinations of noise level and fading level is when $L = 2$ or $L = 3$ hops per symbol are used. In addition, the best coding performance was obtained with the best rate 1/2 convolutional code. The results for the Reed-Solomon codes may not be an accurate representation of their benefit in a bursty channel since burst analysis was not simulated.

B. RECOMMENDATIONS

Further study into other waveform configurations suitable for the LASAT system is needed. This study could include determining the benifits of direct sequence spread spectrum and phase shift keyed (PSK) modulation. Link analysis

must also be performed on the proposed LASAT system. Multiuser interference, and a study of antenna design should be included in the analysis. The fast-frequency-hopping MFSK system theoretically developed in this thesis should perform well in a fading channel with jamming. To confirm the performance results, a hardware simulator implementing this design should be constructed.

Network analysis for the LASAT system should also be studied and should consist of the following tasks:

- Allocating satellite capacity to voice channels in the case where voice is not packetized.
- Design packet protocols to handle a mixture of packetized voice and data traffic.
- Design highly reliable data protocols for priority messages to be used when the link is forced to operate at its threshold.
- Design connectivity algorithm for dynamic crosslinks between LASAT's.

APPENDIX

The unconditional probability density function of z_k can be derived by integrating the conditional pdf over the distribution for a_k such that

$$f_{Z_{1k}}(z_{1k}) = \int_0^\infty f_{Z_{1k}|A_k}(z_{1k}\,|\,a_k) f_{A_k}(a_k) da_k, \tag{A.1}$$

where $f_{Z_{1k}|A_k}(z_{1k}\,|\,a_k)$ and $f_{A_k}(a_k)$ are given by (4.17) and (4.4), respectively. Therefore, the integral to be solved is

$$f_{Z_{1k}}(z_{1k}) = \frac{1}{2\sigma^2}\exp\left\{-\frac{z_{1k}}{2}-\frac{\alpha_k^2}{2\sigma^2}\right\}\int_0^\infty a_k \exp\left\{-a_k^2\left[\frac{1}{2\sigma_k^2}+\frac{1}{2\sigma^2}\right]\right\} \cdot I_0\left[\frac{(z_{1k})^{1/2}a_k}{\sigma_k}\right] I_0\left[\frac{a_k\alpha_k}{\sigma^2}\right] da_k. \tag{A.2}$$

The solution of the integral may be found by using the following indentity from Ref. 17: p. 314

$$\int_0^\infty t e^{-p^2t^2} J_v(at) J_v(bt)\,dt = \frac{1}{2p^2} e^{-(a^2+b^2)/4p^2} I_v\left(\frac{ab}{2p^2}\right), \tag{A.3}$$

where $J_v(x)$ is the Bessel function of the first kind. If it is noted that $I_0(x) = J_0(jx)$, and following substitutions are made

$$\begin{aligned} &t = a_k, \quad v = 0, \\ &p^2 = \left(\frac{1}{2\sigma_k^2}+\frac{1}{2\sigma^2}\right) \\ &a = j\frac{(z_{1k})^{1/2}}{\sigma_k}, \quad b = j\frac{\alpha_k}{\sigma^2}, \end{aligned} \tag{A.4}$$

the result is

$$f_{Z_{1k}}(z_{1k}) = \frac{1}{2(1+2\sigma^2/2\sigma_k^2)} \exp\left\{ - \frac{z_{1k} + \frac{\alpha_k^2}{\sigma_k^2}}{2(1+2\sigma^2/2\sigma_k^2)} \right\} I_0\left[\frac{(z_{1k})^{1/2} \frac{\alpha_k}{\sigma_k}}{(1+2\sigma^2/2\sigma_k^2)} \right] \quad (A.5)$$

This equation can be put into a more convienent format if the substitutions of $\rho_k = \alpha_k^2 R = \alpha_k^2/2\sigma_x^2$ and $\beta = 2\sigma^2 R = 2\sigma^2/2\sigma_k^2$ are made

$$f_{Z_{1k}}(z_{1k}) = \frac{1}{2(1+\beta)} \exp\left\{ - \frac{z_{1k} + 2\rho_k}{2(1+\beta)} \right\} I_0\left[\frac{(z_{1k})^{1/2}(2\rho_k)^{1/2}}{(1+\beta)} \right], \quad (A.6)$$

where ρ_k is the output signal-to-noise ratio of the specular (direct) component, and β is the output signal-to- noise ratio of the diffuse component.

LIST OF REFERENCES

1. Binder, R., Huffman, S. D., Gurantz, I., and Vena, P. A., "Crosslink architectures for a multiple satellite system," *Proc. of IEEE*, Vol. 75, pp. 74-81, Jan. 1987.

2. Stein, S., "Fading channel issues in system engineering," *IEEE J. Select. Areas Commun.*, Vol. SAC-5, pp. 68-88, Feb. 1987.

3. Perakis, J. G., *Digital Communications, 2nd, ed.*, McGraw-Hill, New York, 1989.

4. Whalen, A. D., *Detection of Signals in Noise*, Academic Press, Inc., San Diego, California, 1971.

5. Lee, J. S., Miller, L. E., and French, R. H., "Uncoded peformance for certain ECCM receiver design strategies for multihops symbol FH/MFSK waveforms," *IEEE J. Select. Areas Commun.*, Vol. SAC-3, pp. 611-621, Sept. 1985.

6. Larson, H. J., *Introduction to Probability Theory and Statistical Inference, 2nd ed.*, John Wiley and Sons, Inc., New York, 1974.

7. Feller, W., *An Introduction to Probability Theory and Its Applications, 3rd ed.*, John Wiley and Sons, Inc., New York, 1968.

8. Stark, H., and Woods, J. W., *Probability, Random Processes, and Estimation Theory for Engineers*, Prentice-Hall, Englewood Cliffs, New Jersey, 1986.

9. Lindsey, W. C., "Error probabilities for Rician fading multichannel reception of binary and N-ary signals," *IEEE Trans. on Infor. Theory*, Vol. IT-10, pp. 339-350, Oct. 1964.

10. Lee, J. S., French, R. H., and Miller, L. E., "Error-correcting codes and nonlinear diversity combining against worst case partial-band noise jamming of FH MFSK systems," *IEEE Trans. Commun.*, Vol. COM-36, pp. 471-478, Apr. 988.

11. Campbell, G. A., and Foster, R. M., *Fourier Integrals for Practical Applications*, Van Nostrand, Princeton, New Jersey, 1954.

12. Henrici, P., *Applied and Computational Complex Analysis*, John Wiley and Sons, Inc., New York, 1974.

13. Ha, T. T., *Digital Satellite Communications*, McMillian, New York, 1986.

14. Lee, J. S., Miller, L. E., and Kim, Y. K., "Probability of error analysis of a BFSK frequency-hopping system with diversity under partial-band jamming interference-part II: Performance of square-law nonlinear combining soft decision receivers," *IEEE Trans. Commun.*, Vol. COM-32, pp. 1243-1250, Dec. 1984.

15. Oldenwalder, J. P., "Optimal decoding of convolutional codes", Ph.D. dissertation, Univ. California, Los Angeles, 1970 (Univ. Microfilms 70-19, 875).

16. Hagenauer, J., and Lutz, E., "Forward error correction coding for fading compensation in mobile satellite channels," *IEEE J. Select. Areas Commun.*, Vol SAC-55, pp. 215-225, Feb. 1987.

17. Luke, Y. L., *Integrals of Bessel Functions,* McGraw-Hill, New York, 1962.

INITIAL DISTRIBUTION LIST

		No. Copies
1.	Defense Technical Information Center Cameron Station Alexandria, VA 22304-6145	2
2.	Library, Code 0142 Naval Postgraduate School Monterey, CA 93943-5002	2
3.	Chairman, Code 62 Department of Electrical and Computer Engineering Naval Postgraduate School Monterey, CA 93943-5000	1
4.	Commander Naval Space Command Attn: Code N3 Dahlgren, VA 22448	1
5.	Commander United States Space Command Attn: Technical Library Peterson Air Force Base, CO 80914	1
6.	Chief of Naval Operations Attn: Naval Space Systems Division (OP943) Washington, DC 20305-2000	1
7.	Professor Tri T. Ha, Code 62Ha Department of Electrical and Computer Engineering Naval Postgraduate School Monterey, CA 93943-5000	5
8.	Professor Glen A. Myers, Code 62Mv Department of Electrical and Computer Engineering Naval Postgraduate School Monterey, CA 93943-5000	1
9.	Lieutenant Thomas M. Clemons, III 7629 S. River Rd. Marine City, MI 48039	2